APPLICATIONS OF STATISTICAL ANALYSIS TECHNIQUES FOR NEUROIMAGING DATA: RANDOMIZED SINGULAR VALUE DECOMPOSITION FOR PARTIAL LEAST SQUARES ANALYSIS AND THIN PLATE SPLINES FOR SPATIAL NORMALIZATION

by

Bedda Lynn Rosario-Rivera

BS, University of Puerto Rico, 1999

MPH, University of Puerto Rico, 2000

Submitted to the Graduate Faculty of

Department of Biostatistics

Graduate School of Public Health in partial fulfillment

of the requirements for the degree of

Doctor of Philosophy

University of Pittsburgh

2008

UNIVERSITY OF PITTSBURGH

Graduate School of Public Health

This dissertation was presented

by

Bedda Lynn Rosario-Rivera

It was defended on

November 21, 2008

and approved by

Dissertation Advisor: Lisa Weissfeld, Ph.D.
Professor
Department of Biostatistics
Graduate School of Public Health
University of Pittsburgh

Committee Member: Julie Price, Ph.D.
Associate Professor
Department of Radiology
School of Medicine
University of Pittsburgh

Committee Member: Sati Mazumdar, Ph.D.
Professor
Department of Biostatistics
Graduate School of Public Health
University of Pittsburgh

Committee Member: Stewart Anderson, Ph.D.
Professor
Department of Biostatistics
Graduate School of Public Health
University of Pittsburgh

APPLICATIONS OF STATISTICAL ANALYSIS TECHNIQUES FOR NEUROIMAGING DATA: RANDOMIZED SINGULAR VALUE DECOMPOSITION FOR PARTIAL LEAST SQUARES ANALYSIS AND THIN PLATE SPLINES FOR SPATIAL NORMALIZATION

Bedda Lynn Rosario-Rivera, Ph.D.

University of Pittsburgh, 2008

This dissertation applies two statistical analysis techniques for neuroimaging data. The first aim of this dissertation is to apply randomized singular value decomposition for the approximation of the top singular vectors of the singular value decomposition of a large matrix. Randomized singular value decomposition is an algorithm that approximates the top k singular vectors of a matrix given a subset of its rows or columns. Several statistical applications, such as partial least squares, require the computation of the singular value decomposition of a matrix. Statistical packages have built in functions that can compute the singular value decomposition of a matrix. In many applications, however, computing the SVD of a matrix is not possible because computer memory requirements associated with matrix allocation is high, limiting its use in high-dimensional settings. Neuroimaging studies can generate measurements for hundreds of thousands of voxels from an image. Therefore, performing partial least squares analysis on these datasets is not possible using statistical packages. Simulation studies showed that the randomized singular value decomposition method provides a good approximation of the top singular vectors and therefore a good approximation of the partial least squares summary scores. This method is significant for public health since it allows researchers to perform statistical analysis at a voxel level with only a sample of a large dataset.

The second aim is to apply a thin plate spline method for spatial normalization of structural magnetic resonance images. Spatial normalization is the process of standardizing

images of different subjects into the same anatomical space. The idea behind this procedure is to match each data volume from a subject to a template, so that specific anatomic structures will occupy the same voxels. Spatial normalization is a critical step in the analysis of brain imaging data since it produces the "raw" data for subsequent statistical analyses.

TABLE OF CONTENTS

LIST OF TABLES

LIST OF FIGURES

ACKNOWLEDGEMENTS

I would like to express my sincere gratitude to my committee chair, Dr. Lisa Weissfeld, for her guidance, patience, and support throughout the process of preparing my dissertation. I would also like to thank my committee members, Dr. Julie Price, Dr. Sati Mazumdar and Dr. Stewart Anderson for their support, guidance and helpful suggestions. In addition, I would like to thank my colleague and friend Wenzhu Bi for all her help and support.

I owe a huge debt of gratitude to my parents Osvaldo and Bedda, my brothers Carlos and Luis and my sister Militza for their love, support and encouragement throughout my Ph.D. and throughout my life, and for always believing in me.

Lastly, but most important I would like to thank my husband and best friend Emilio, for his love, support, patience and understanding during this process. I would not have done this dissertation without him.

1.0 INTRODUCTION

The problem of applying statistical analysis methods to high dimensional data has become more important recently as researchers find ways to process large amounts of information. Research in neuroimaging and many other areas has resulted in the generation of large amounts of data that are of high dimension. The need for approaches that facilitate the application of statistical analysis methods to high dimensional data has thus become important. McIntosh et al. introduced partial least squares (PLS) for the analysis of functional neuroimaging data in 1996. They showed that PLS analysis deals efficiently with datasets that have many variables that are highly correlated (e.g. neuroimaging data). After this first application, several studies have applied PLS for the analysis of neuroimaging data (Xu et al., 2007; McIntosh et al., 2004; Nestor et al., 2002; Lobaugh et al., 2001). PLS is a multivariate data analysis technique that generalizes and combines features from multiple regression and principal component analysis. The goal of this technique is to search for a set of latent variables that performs a simultaneous decomposition of blocks of observed variables, X and Y, with the constraint that these components maximize the covariance between the blocks using the fewest dimensions. A PLS analysis requires the computation of the covariance matrix between X and Y, followed by the computation of the singular value decomposition of this matrix in order to explain the cross-correlation between X and Y. Most neuroimaging studies define block X as the design matrix, which contains vectors of contrasts defining the experimental design and/or behavioral

measurements and block Y as a matrix that contains region-of-interest (ROI) measurements or normalized functional image data, for all subjects and all experimental conditions, for a particular image modality. However, when comparing two sets of voxel-based functional neuroimaging data, the computation of the singular value decomposition can be infeasible since it requires large amounts of memory, which is not generally readily available on a computer. We proposed the application of the randomized singular value decomposition method, developed in the image-processing field by Drineas et al. (2004), for the approximation of the top k singular vectors of a matrix, and therefore approximation of PLS summary scores. Randomized singular value decomposition is an algorithm that approximates the top k singular vectors of a matrix given a subset of its rows or columns. This algorithm will make the problem more manageable, though still limited by high dimensionality.

Voxel-based analysis of neuroimaging data takes into account every voxel in the brain. Therefore, spatial normalization must be applied to every subject's image so that specific anatomic structures will occupy the same voxels. Spatial normalization is an essential imaging pre-processing step for voxel-based analyses of brain data since it produces the "raw" data for subsequent statistical analyses. This step ensures that data from different subjects are derived from homologous regions in the brain. Several methods are available to perform this process. The most widely used software for spatial normalization in the research literature is Statistical Parametric Mapping (SPM). Assessment of the spatial normalization process in SPM was conducted in a study that was published in the journal NeuroImage (Rosario et al., 2008). The purpose of this study was to assess the effect of different parameter settings for spatial normalization, standard and unified methods, in SPM5. Even though, spatial normalization in SPM is widely used, it requires manual tuning of the parameter estimates for spatial

normalization. In this dissertation research, we proposed to investigate two methods for spatial normalization of magnetic resonance imaging that did not require a high degree of manual intervention. These methods were interpolation thin plate spline and smoothing thin plate spline. The thin plate spline method is an effective tool for modeling coordinate transformations. The advantages of interpolation thin plate spline and smoothing thin plate spline methods are that these do not require manual tuning. In addition, these methods can be significantly faster than other spatial normalization methods that are already available.

1.1 OBJECTIVES

The purpose of this dissertation is to consider using statistical methods to extend the feasible applications of RSVD and thin plate splines to allow for routine applications in clinical settings. First, we extend the method of PLS to reduce the computational burden by applying randomized singular value decomposition as an approximation of the singular value decomposition and therefore an approximation of the summary scores. Second, we propose a method for linear and nonlinear transformation of structural magnetic resonance image data using thin plate splines, which is an extension of the current methods for normalization. In addition, we present results from a study that was performed to assess and compare the parameter settings for spatial normalization in Statistical Parametric Mapping (SPM) and was published in the journal NeuroImage.

1.2 SUMMARY

The layout of the dissertation will be as follows. Chapter 2 provides the reader with general background information on concepts related to neuroimaging data discussed in this dissertation. Chapter 3 will present the algorithm of randomized singular value decomposition (RSVD) for the approximation of the top singular vectors of a large matrix. In Chapter 4, we describe partial least squares as a multimodality analysis technique to determine the relationship between two imaging tracers: [^{11}C]Pittsburgh Compound B and [^{18}F]Fluoro-2-deoxy-D-glucose positron emission tomography (PET) data. In addition, we demonstrate how the proposed RSVD approximation method can be applied to partial least squares analysis. Chapter 5 will discuss results from a study that was performed to evaluate and compare the parameter settings for spatial normalization in Statistical Parametric Mapping (SPM) and was published in the journal NeuroImage. Chapter 6 will present a thin plate spline method for linear and nonlinear transformation of magnetic resonance imaging data.

2.0 NEUROIMAGING AND SPATIAL NORMALIZATION

This chapter provides the reader with general background information on concepts related to neuroimaging data discussed on this dissertation. This work assumes that the reader has some level of familiarity with these concepts.

2.1 NEUROIMAGING

2.1.1 Neuroimaging

Neuroimaging is the application of imaging techniques to image the structure or function of the brain in living humans. Neuroimaging can be divided into two categories: structural imaging and functional imaging. Structural imaging deals with the structure of the brain and can be used in clinical applications for the diagnosis of intracranial diseases (e.g. tumor). This category includes several imaging techniques such as Magnetic Resonance (MR) imaging and Computed Tomography (CT) imaging. Functional imaging can be applied to measure brain function as it relates to neurobiological processes and/or performance of cognitive tasks in specific areas of the brain. Several functional imaging techniques include functional Magnetic Resonance Imaging (fMRI), Single Photon Emission Computed Tomography (SPECT) and Positron Emission Tomography (PET). This work will focus on structural MR and functional PET imaging.

2.1.2 Structural Magnetic Resonance Imaging

Magnetic Resonance (MR) imaging is a non-invasive medical imaging technique used to produce high quality two- and three-dimensional structural or functional images of the inside of the human body. This technique provides detailed images of the body in any plane and a high degree of anatomical detail. In clinical settings, an MR image is primarily used to distinguish pathologic tissues (e.g. tumor) from normal tissue. MR imaging uses magnetic fields and radio waves to produce these images. Figure 1 shows a sagittal view of a structural magnetic resonance image.

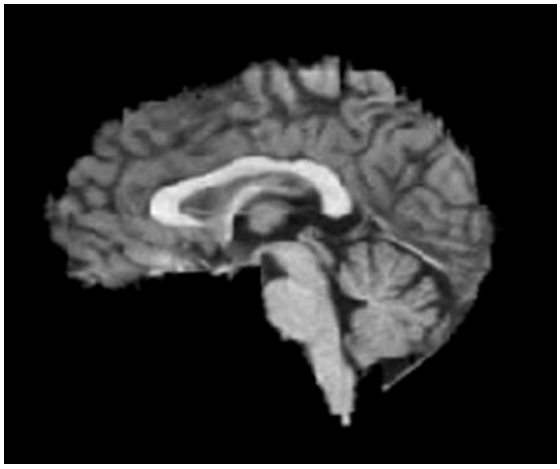

Figure 1 Sagittal view of a structural magnetic resonance image of the brain for a control subject (56 years old).

2.1.3 Positron Emission Tomography

Positron emission tomography (PET) is an imaging technique used to produce a three dimensional image or a map of functional processes in the body ("Positron emission

tomography," 2008). It is designed to provide information about chemical activity within certain organs and tissues. This imaging technique is useful in evaluating normal function and a variety of conditions such as neurological diseases, heart diseases and cancer among others. PET scanning has been used to provide visual images of activity in the brain when a person is performing a task (e.g. read, talk or listen to music). In addition, PET can be used as a tool to differentiate Alzheimer's disease from other types of dementia disorders, such as frontal temporal dementia and Huntington's disease.

During a PET scan, a radioactive tracer is injected intravenously in the person's arm. A radioactive tracer is a substance that contains a radioisotope. These tracers are used to measure the rate of a chemical process and to track the movement of a substance through the cells or tissue ("Radioactive tracer," 2008). The tracer distributes through the body and localizes in a specific organ or tissue, based on the specific properties of the tracer. The radioactive decay of the tracer by positron emission produces photons that are detected by the PET scanner. This information is processed using computational mathematical algorithms that produce images. Several radioactive tracers are available for PET imaging including [^{18}F]Fluoro-2-deoxy-D-glucose and [^{11}C]Pittsburgh Compound B.

2.1.3.1 [^{18}F]Fluoro-2-deoxy-D-glucose

[^{18}F]Fluoro-2-deoxy-D-glucose (FDG) is a radiotracer that is widely used in PET studies. This radiotracer is an analogue of glucose that reflects cellular metabolism and is take up by those cells in the brain that are more active. The concentration of the tracer in the image shows tissue metabolic activity that is proportional to glucose uptake. After the tracer is injected into a patient, a PET scanner forms images. Several studies (Hoffman, et al., 1989; Minoshima, et al.,

1995; Silverman, 2004 and Bittner, et al. 2005 and others) have applied FDG as a tool for the diagnosis of Alzheimer's disease.

2.1.3.2 [^{11}C]Pittsburgh Compound B

[^{11}C]Pittsburgh Compound B (PIB) is a radiotracer that can be used to image amyloid-beta plaques in neural tissue with PET. This tracer is a fluorescent derivative of the dye Thioflavin T, which is a dye used to visualize plaques composed of amyloid-beta found in the brains of patients with Alzheimer's disease. Amyloid-beta is a peptide of amino acids that is thought to be the main constituent of amyloid plaques in the brain of patients with Alzheimer's disease ("Beta amyloid," 2008).

The first PIB study that included human subjects with a clinical diagnosis of Alzheimer's disease was performed in February 2002 at the Uppsala University in Sweden. This initial study was then extended to include sixteen Alzheimer's disease subjects and nine healthy controls. Results from this study showed that PIB retention in cortical areas was 2-fold greater for Alzheimer's disease subjects when compared to control subjects (Klunk, et al., 2004). These areas are known to contain amyloid in Alzheimer's disease subjects. Results also showed that no group differences were found in areas that are free of amyloid in Alzheimer's disease subjects. Following this initial study, PIB has been widely used to conduct trials in human subjects (Price, et al., 2005; Klunk, et al., 2007). Figure 2 shows an axial view for PIB PET (top) and FDG PET (bottom) image scan for a control and an Alzheimer's disease (AD) subject. The top figure shows strong PIB binding in Alzheimer's disease and non-specific uptake of PIB in controls. The bottom figure shows normal metabolism in controls and lower metabolism in Alzheimer's disease, specifically in the parietal region.

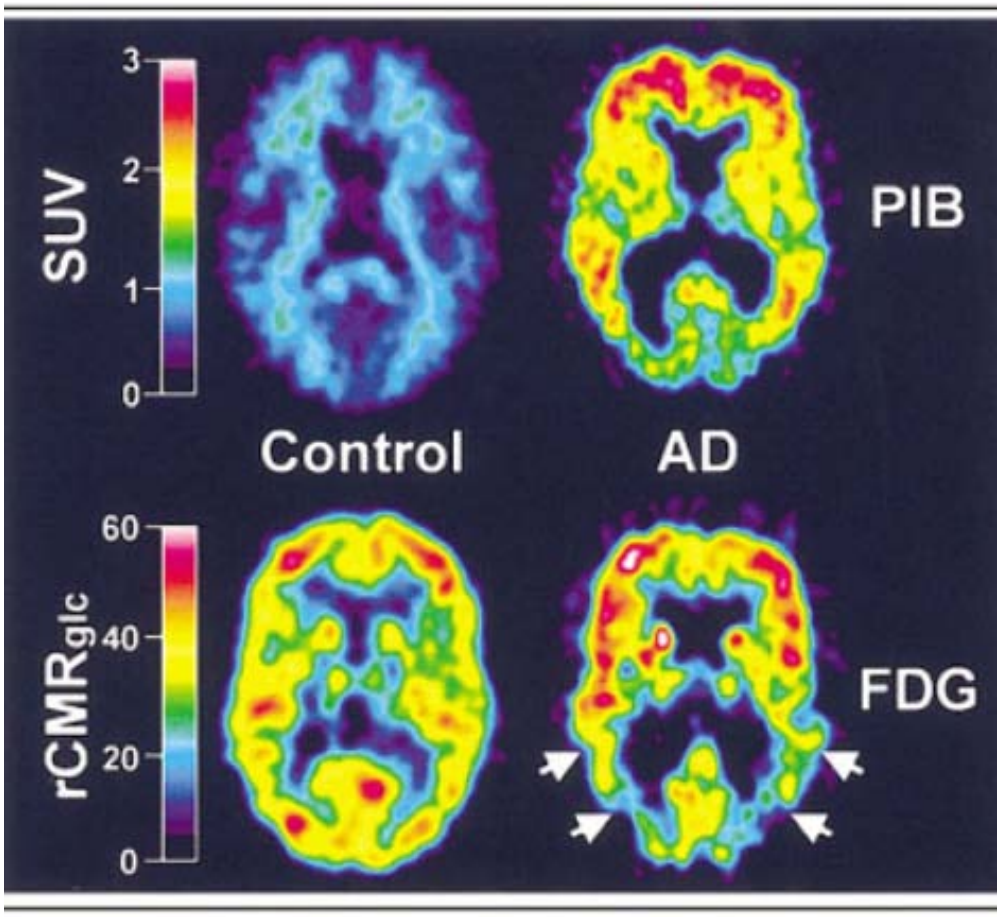

Figure 2 PIB PET and FDG PET image scans for a control (left) and an Alzheimer's disease (right) subjects. Source: Klunk et al. (2004).

2.1.4 Multimodality

Multimodality refers to the involvement or combination of different radioactive tracers (e.g. FDG versus PIB) or different imaging techniques (e.g. MR versus PET).

2.2 ANALYSIS OF NEUROIMAGING DATA

The analysis of neuroimaging data can be performed on a region-of-interest or on a voxel-based basis.

2.2.1 Region-of-interest Analysis

A region-of-interest (ROI) is an anatomical region that is drawn on a magnetic resonance image by hand or automatically by using specialized software. The aim of defining ROIs is to calculate the average of the studied parameter in a specific anatomical region (e.g. quantification of PIB binding in precuneus). This type of analysis is performed to determine if a specific region of the brain has been activated. After defining a region, a statistical analysis is performed on the mean value of the voxels within a region. This type of analysis has proven to be very powerful in analyzing the radioactivity in well defined regions. Region-of-interest analyses have two main advantages: statistical power and simplicity of interpretation of results, relative to voxel-based analyses. The outcome measure for this analysis is amyloid-beta deposition or glucose metabolism for a region.

2.2.2 Voxel-based Analysis

Voxel-based analyses of neuroimaging data take into account every voxel in the image. Before performing this analysis, spatial normalization must be applied to every subject's image so that specific anatomic structures occupy the same voxels. The outcome measure for this analysis is amyloid-beta deposition or glucose metabolism for each voxel.

2.3 SPATIAL NORMALIZATION

Spatial normalization is the process of applying a spatial transformation that moves and warps images from a number of subjects so that they map onto the same coordinate system or standard anatomical space defined by a template. The idea behind this procedure is to match each data volume from a subject's image to a template, so that specific anatomic structures will occupy the same voxels. The objective of spatial normalization is to remove unwanted differences between the subjects' images to allow subsequent analysis of the data. Spatial normalization typically involves rotations, translations, and nonlinear warping of the brain image to match a standard template. Image warping is an essential pre-processing step for voxel-based analyses of brain data because it produces the "raw" data for subsequent statistical analyses. This step ensures that data from different subjects are derived from homologous regions in the brain. Several methods are available to perform this process. Statistical Parametric Mapping (SPM) is the most widely used software for spatial normalization in the research literature.

Spatial normalization methods can be grouped into two categories: intensity-based or label-based. Intensity-based methods identify a spatial transformation that optimizes some voxel similarity measure between the source and the reference image. The label-based approaches identify homologous features, such as points, lines or surfaces, in the source and reference image and finds the transformation that best superimpose them. This work will focus on a label-based approach.

3.0 RANDOMIZED SINGULAR VALUE DECOMPOSITION

3.1 INTRODUCTION AND PROBLEM DESCRIPTION

Singular value decomposition (SVD) is an important and useful tool for factorization of a rectangular matrix. It is widely applied in statistics, signal processing and pattern recognition. In statistics, it is applied in several methods such as partial least squares and principal component analysis. Statistical or mathematical packages (e.g. R Software and MATLAB) have built in functions that can compute the SVD of a matrix. In many applications, however, computing the SVD of a matrix is not possible because computer memory requirements associated with matrix allocation is high, limiting its use in high-dimensional settings. Neuroimaging studies can generate measurements for hundreds of thousands of voxels from an image. Therefore, computing the SVD of an extremely large matrix using either statistical or mathematical packages can be infeasible for routine applications in clinical settings. The goal of this chapter is to present an approach, randomized singular value decomposition, which can be used to approximate the top k singular vectors of a large matrix. Drineas et al. (2004) developed this method in image processing for approximating the top k singular vectors of a matrix given a subset of its rows or columns.

This chapter is presented as follows. In Section 3.2, the singular value decomposition is defined. Section 3.3 presents the method for approximating the SVD of a matrix. Implementation and results are presented in Chapter 4.

3.2 SINGULAR VALUE DECOMPOSITION REVIEW

The singular value decomposition (SVD) is a tool for factorization of a rectangular matrix. It is widely applied in signal processing and statistics. The SVD of a $m \times n$ matrix S is defined by:

$$S = U \cdot \Sigma \cdot V^T, \tag{3.1}$$

where U is an $m \times m$ orthogonal matrix, Σ is an $m \times n$ matrix with nonnegative numbers on the diagonal and zeros off the diagonal, V is an $n \times n$ orthogonal matrix, and V^T denotes the transpose matrix of V. The columns of U are called the left singular vectors or orthonormal eigenvectors of $S \cdot S^T$. The rows of V^T are called the right singular vectors or orthonormal eigenvectors of $S^T \cdot S$. The elements of Σ are called the singular values.

A matrix M is orthogonal if $MM^T = M^T M = I$, where I is the identity matrix. The identity matrix is a square matrix with entries on the diagonal equal to 1 and all other entries equal to zero. A matrix N is orthonormal if each row of N is a unit vector and if the dot product of each vector with each other vector is zero. A unit vector is a vector whose length is one. A dot product of two vectors $a = (a_1, \ldots, a_n)$ and $b = (b_1, \ldots, b_n)$ is defined as $a \cdot b = \sum_{i=1}^{n} a_i b_i = a_1 b_1 + \cdots + a_n b_n$. Singular values and singular vectors are also known as latent roots and latent vectors, respectively.

3.3 APPROXIMATING TOP k SINGULAR VECTORS

This section presents an algorithm for the approximation of the top k singular vectors of a matrix. This algorithm, randomized singular value decomposition, is based on randomly sampling either the rows or columns of the matrix and computing the SVD of the reduced matrix.

3.3.1 Randomized Singular Value Decomposition

Randomized singular value decomposition (RSVD) is an algorithm that approximates the top k singular vectors of a matrix given a subset of its rows or columns. Drineas et al. (2004) introduced this method for image processing. The RSVD algorithm samples a constant number of rows (or columns) of the matrix, scales them appropriately to form a small matrix U, and then computes the SVD of U to provide an approximation of the top k right (or left) singular vectors of the original matrix.

Given an $m \times n$ matrix S, the algorithm works as follows:

1. Pick r rows of S and define an $r \times n$ matrix U.

   for($t = 1$ to r)

   Pick an integer from $\{1, \ldots, m\}$, where Prob(pick i) = p_i and $\sum_{i=1}^{m} p_i = 1$.

   Include $\frac{S^{(i)}}{\sqrt{r \cdot p_i}}$ as a row of U, where $S^{(i)}$ denotes the ith row of S.

2. Compute $U \cdot U^T$ and compute its singular value decomposition.

3. Return the right singular vectors of U by defining an $n \times k$ matrix H with columns defined by $h^{(t)} = \frac{U^T w^{(t)}}{\left| U^T w^{(t)} \right|}$, where $w^{(t)}$ are the left singular vectors of U and $t = 1, \ldots, k$.

The $h^{(t)}$ are the approximations to the top k right singular vectors of S. The sampling process to select the rows (or columns) can be with or without replacement, as explained in Drineas, et al. (2004). This algorithm can be used to approximate the top k singular vectors of a considerably large matrix. The RSVD method will be applied in Chapter 4.

3.3.2 Sampling Process

The sampling process used to select the rows from matrix S is a weighting sampling method with replacement, where the sampling weights p_i are defined as

$$p_i = \frac{\left| S^{(i)} \right|^2}{\left\| S \right\|_F^2}, \tag{3.1}$$

where $\left| S^{(i)} \right|$ defines the norm of each row of the matrix S, $\left\| S \right\|_F^2 = \sum_{i,j} S_{ij}^2$, $i = 1 \ldots m$ and $j = 1 \ldots n$.

4.0 MULTIMODALITY ANALYSIS TECHNIQUES

4.1 INTRODUCTION

Dementia is a brain disorder that affects a person's ability to carry out regular daily activities. The most common form of dementia among older people is Alzheimer's disease. Therefore, Alzheimer's disease (AD) has become an important public health problem. Several hypotheses have been stated to explain the cause of Alzheimer's disease. One of these hypothesis states that amyloid-beta (Aβ) deposition is a central causative factor of the disease. Currently, the diagnosis of AD is based on the presence of amyloid-beta plaques and neurofibrillary tangles in cortical regions in the brain at autopsy. Therefore, measurement of amyloid-beta plaques in human subjects could help identify the possible causes, diagnosis and treatment of AD.

Several imaging techniques have been applied for the study of Alzheimer's disease, mainly positron emission tomography (PET). Several imaging tracers have been used for these studies including FDG and PIB. Currently, FDG is the most commonly used imaging tracer for PET. This tracer is widely used for the assessment of glucose metabolism in the brain. Several studies have applied FDG as a tool for the diagnosis of AD such as Hoffman, et al., 1989; Minoshima, et al., 1995; Silverman, 2004 and Bittner, et al. 2005 among others. PIB was developed as an imaging agent to image amyloid-beta plaques in neural tissue. Results from the

first human PIB PET study showed that PIB retention in cortical areas was 2-fold greater for AD subjects when compared to control subjects (Klunk, et al., 2004).

It is important to study and understand the independent and combined information that these different radiotracers provide about the disease process. Several techniques, such as partial least squares (PLS) have been shown to be a useful multivariate tool for neuroimaging data (e.g. McIntosh et al., 1996). This technique combines features from multiple regression analysis and principal component analysis. It is used to determine the relationship between two sets of correlated measures when the subject sample is small, and it is particularly useful when dealing with large datasets. This technique requires the singular value decomposition (SVD) of a matrix. One of the challenges is to develop effective ways for the computation of the SVD of a matrix when working with large datasets.

The aim of this work is the application of PLS to determine the relationship between FDG and PIB in terms of functional voxel-based image data. In addition, we would like to assess group differences across three different subject groups: control (CT), Alzheimer's disease (AD) and mild cognitive impairment (MCI). MCI may be a precursory state to AD as many MCI subjects develop AD. However, FDG and PIB functional image data is composed of hundreds of thousands of voxels from every image. Statistical software packages are limited in the calculations they can perform by the amount of physical memory that is available in the computer on which they run. Performing PLS analysis on the functional voxel-based dataset for the whole brain will require large amounts of memory, which is not readily available on a computer for routine clinical applications. Therefore, performing PLS analysis on this dataset (FDG and PIB functional image data at the voxel level) was not feasible for the work in this

dissertation, due to these memory constrains. However, by using randomized singular value decomposition (RSVD), as explained in Chapter 3, we can approximate the top k singular vectors of a considerably large matrix without having to use the entire dataset, and therefore apply this method to PLS. Before we can apply the RSVD method to the voxel-based data for the whole brain, we need to be able to verify that the approximation works.

In order to validate the RSVD approximation, we will take an inductive approach. This approach will consist of first applying the PLS analysis to a small dataset and comparing the results to those obtained from PLS analysis using RSVD. If the results are similar, then, we will apply the same analyses to a larger dataset that is within the memory constraints of this work. If we can prove that our approach works for the small dataset, and with the larger dataset, then we will induce that applying RSVD to PLS analysis will work for the larger dataset, which cannot be computed due to memory constraints.

This chapter is presented as follows. In Section 4.2 we present a literature review. In Section 4.3, we present a review of the PLS method. Implementation and results of PLS analysis and RSVD application to PLS analysis are presented in Section 4.4. Conclusions and discussion are presented in Section 4.5.

4.2 LITERATURE REVIEW

Partial least squares (PLS) is a multivariate data analysis technique that generalizes and combines features from multiple regression and principal component analysis. Herman Wold (1975) developed it for the social sciences, specifically in economics. McIntosh et al. introduced

it to functional MR neuroimaging data (voxel-based) in 1996. They showed that PLS analysis deals efficiently with datasets that have many variables that are highly correlated. After this first application, several studies have applied PLS for the analysis of neuroimaging data (Xu et al., 2007; McIntosh et al., 2004; Nestor et al., 2002; Lobaugh et al., 2001). However, none of these studies applied PLS to determine the relationship between two types of functional image data (voxel level).

4.3 PARTIAL LEAST SQUARES ANALYSIS REVIEW

PLS is a multivariate data analysis technique that searches for a set of latent variables that performs a simultaneous decomposition of blocks of observed variables, X and Y, with the constraint that these components maximize the covariance between the blocks using the fewest dimensions. PLS deals efficiently with datasets that have many variables that are highly correlated (e.g. neuroimaging data).

Most neuroimaging studies define block X as the design matrix, which contains vectors of contrasts defining the experimental design and/or behavioral measurements and block Y as a matrix that contains region-of-interest (ROI) measurements or normalized functional image data, for all subjects and all experimental conditions, for a particular image modality. The block Y consists of one row per subject. The block X might also be defined as ROI measurements or normalized functional image data, for all subjects and all experimental conditions, for an image modality different from block Y. After defining the blocks, a cross-correlation matrix S of X by Y is calculated. The elements S_{ij} are the covariance of X_i with Y_j. The cross-correlation relates the pixels of a normalized image (or ROI measures) to the design/behavioral measures

matrix. It can also relate pixels of a normalized functional image (or ROI measures) of an image modality to pixels of a normalized image (or ROI measures) from another image modality. Then, a singular value decomposition of the matrix S is performed to analyze the cross-correlation matrix. The result of this decomposition is a series of paired singular vectors (or latent variables) and singular values. The paired latent variables provide two sets of weights or "saliences"; one set of weights corresponding to each measure in block X and one set corresponding to each measure in block Y. The singular values define the covariance between the singular vectors and are used to calculate the proportion of covariance accounted for by a pair of latent variables. The last step is to calculate summary scores. These scores express the original data in terms of components along the singular vectors. That is, the summary scores provide an overall value for each latent variable determined for each subject. The summary scores are the dot product of subject's region-of-interest measure (or voxel value) and the weights for a particular latent variables. Singular images can also be obtained from PLS results. These singular images reflect pixels from a particular image modality most (or least) sensitive to a contrast or behavioral measure.

4.4 IMPLEMENTATION

4.4.1 Human Subjects and Demographic Variables

Seventy-four control, twenty-eight mild cognitive impairment and twenty Alzheimer's disease subjects were recruited for an FDG PET and PIB PET imaging study. Subject characteristics are provided in Table 1 including age, gender and Mini Mental State Examination (MMSE). MMSE

is a 30-point questionnaire that is commonly used to screen for dementia. Any score above 27 is effectively normal; between 20 and 26 indicates mild dementia; between 10 and 19 indicates moderate dementia, and below 10 indicates severe dementia (Folstein et al., 1975). Most subjects were recruited and evaluated at the University of Pittsburgh Alzheimer's Disease Research Center (ADRC). Some control subjects were recruited through a linked study of amyloid deposition in normal aging (R37 AG025516, Klunk). Informed consent was obtained for all subjects through an IRB approved consent process including the ADRC protocol and the PET imaging protocol (IRB protocols: #0403007, #0412004, #0506015, #0501007, #0411040)

.

Table 1 Subject Characteristics

Group	Age (mean ± SD, yrs)	Gender (M:F)	MMSE (mean ± SD)
Control ($n = 74$)	71.6 ± 9.0	25:49	29 ± 2
MCI ($n = 28$)	69.8 ± 7.9	21:7	27 ± 3
AD ($n = 20$)	70.9 ± 9.4	14:6	22 ± 4

4.4.2 Magnetic Resonance, Fluorodeoxyglucose and Pittsburgh Compound B Imaging

Magnetic resonance (MR) imaging was performed using a 1.5 T GE Signa scanner. A volumetric spoiled gradient recalled (SPGR) sequence with parameters optimized for contrast among gray matter, white matter, and cerebrospinal fluids were acquired in the coronal plane (TE/TR=5/25, flip angle=40°, NEX=1, slice thickness=1.5mm/0mm interslice). The SPGR data were acquired to define region-of-interest (ROI), perform spatial normalization and for volume correction of the PET imaging data (see Price et al., 2005; Ziolko et al., 2006).

FDG was synthesized using the standard method of Hamacher et al. (1986). PIB was synthesized using the simplified method of Wilson et al. (2004). The PET data were acquired using a Siemens/CTI ECAT HR+ scanner (3D mode, 15.2 cm field of view, 63 planes, reconstructed image resolution ~6mm) fitted with a Neuro-insert (CTI PET Systems, Knoxville, TN, USA) to reduce scatter (Weinhard, 1998). Data were reconstructed using filtered back projection and corrected for attenuation (^{68}Ge/^{68}Ga rods), scatter (Watson 2000), and radioactive decay. A thermoplastic mask immobilization unit was used to minimize head motion during the scan. PIB was injected intravenously (10-15 mCi over 20 sec, specific activity ~ 1.5 Ci/μmol) and dynamic PET scanning (34 frames) was performed over 90 minutes. FDG was administered (5mCi) about two hours after the start of the PIB scan and a 35 min uptake period as explained in Lopresti et al. (2005) and Ziolko et al. (2006).

Each subject's co-registered MR scan was spatially normalized to the elderly template in SPM. The elderly structural template was created in-house using images from 419 healthy subjects (69 ± 7.5 years) (Spears et al., 2005). Spatial normalization was performed using SPM software (Wellcome Department of Imaging Neuroscience, London, UK, 2007) with the default parameter settings. Each subject's transformation parameters were then applied to FDG and PIB parametric images. All normalized images were written out using the template bounding box and voxel size of 4 mm (dimensions of the functional image data was 47 x 56 x 46). Prior to analysis, each spatially normalized FDG and PIB image was smoothed using a 12mm FWHM Gaussian isotropic kernel.

Following successful image co-registration, region-of-interest will be defined on each individual's transformed MR image and transferred to the PET data for sampling over multiple contiguous planes and several regions will be defined. ROIs will be applied to the dynamic PET

data to obtain regional time-activity data (*Ci/ml) based upon a calibrated phantom standard. Data will be analyzed using the Logan graphical method (Logan et al. 1996) to obtain measures of the total PIB distribution volume (VT). Regional VT measures will be normalized to the VT value obtained in the nondisplaceable binding reference region (i.e., cerebellum, VND) to minimize the non-specific effects. This measure is the distribution volume ratio (DVR) and is the outcome measure of PIB retention. The FDG data are summed over 40 to 60 min post-injection (4 frames). Regional FDG uptake values will be normalized to the summed cerebellar value determined using each individual's MR-based cerebellar ROI to sample the co-registered summed FDG PET image for that individual. This provided FDG standardized uptake value ratio (SUVR). Detailed PET methods can be found in Price et al. (2005).

Seventeen region-of-interest (ROI) were created across multiple planes. Each ROI is a subset of samples within a dataset identified for a particular purpose. The ROIs included dorsal (DFC) and ventral (VFC) frontal cortices; lateral temporal (LTC), mesial temporal (MTC), parietal (PAR) and sensory motor (SMC) cortices; occipital cortex (OCC) and occipital pole (OCP); pregenual (PAC) and subgenual (SAC) anterior cingulate; lower (PCL), middle (PCM) and upper (PCU) precuneus; anterior ventral striatum (AVS); pons (PON); sub-cortical white matter (SWM) and thalamus (THL). The ROI measures, for FDG and PIB, are summarized in Tables 2 and 3, respectively.

Table 2 Region-of-interest measures for FDG.

	FDG SUVR Mean (Standard Deviation)		
Region	Control	MCI	AD
AVS	1.1452 (0.1191)	1.1319 (0.1036)	1.1185 (0.1190)

Table 2 continued

DFC	1.1816 (0.1028)	1.1769 (0.1135)	1.1548 (0.1362)
LTC	1.0516 (0.0692)	1.0331 (0.0915)	0.9221 (0.1091)
MTC	0.7561 (0.0625)	0.7747 (0.0780)	0.7564 (0.0555)
OCC	1.1695 (0.0859)	1.2015 (0.1158)	1.2049 (0.1128)
OCP	1.1474 (0.1049)	1.1502 (0.0917)	1.1156 (0.1292)
PAC	1.0920 (0.0956)	1.1325 (0.1316)	1.1336 (0.1059)
PAR	1.1218 (0.0867)	1.1210 (0.0997)	1.0418 (0.1518)
PCL	1.2505 (0.1041)	1.2179 (0.1098)	1.1266 (0.1390)
PCM	1.2982 (0.1022)	1.2752 (0.1266)	1.1661 (0.1587)
PCU	1.2533 (0.0885)	1.2625 (0.1206)	1.1947 (0.1485)
PON	0.6822 (0.0728)	0.6767 (0.0595)	0.6898 (0.0712)
SAC	1.0823 (0.0936)	1.1124 (0.1139)	1.1064 (0.1087)
SMC	1.2044 (0.0907)	1.2641 (0.1365)	1.2777 (0.0995)
SWM	0.4683 (0.0699)	0.4855 (0.0806)	0.5032 (0.0681)
THL	1.0147 (0.0987)	1.0257 (0.1135)	1.0111 (0.0843)
VFC	1.1519 (0.0994)	1.1472 (0.1056)	1.1113 (0.1188)

Table 3 Region-of-interest measures of PIB retention.

	PIB DVR Mean (Standard Deviation)		
Region	Control	MCI	AD
AVS	1.1884 (0.2018)	1.4684 (0.4016)	1.9659 (0.1550)
DFC	1.3260 (0.2526)	1.6869 (0.4798)	2.3513 (0.1749)
LTC	1.1995 (0.1933)	1.4948 (0.4018)	2.0890 (0.1695)
MTC	1.0629 (0.0978)	1.2035 (0.1686)	1.3365 (0.1080)
OCC	1.2305 (0.1423)	1.3617 (0.2514)	1.6867 (0.2088)
OCP	1.2154 (0.1529)	1.3942 (0.2936)	1.7437 (0.2245)
PAC	1.3330 (0.2917)	1.7687 (0.5720)	2.5175 (0.2089)
PAR	1.2818 (0.2138)	1.5664 (0.4079)	2.1113 (0.1843)

Table 3 continued

PCL	1.2622 (0.2651)	1.5929 (0.4574)	2.2776 (0.2388)
PCM	1.3155 (0.2754)	1.6887 (0.5077)	2.4582 (0.2388)
PCU	1.3549 (0.2886)	1.7249 (0.5207)	2.5296 (0.2421)
PON	1.4856 (0.1265)	1.4573 (0.0941)	1.4417 (0.0915)
SAC	1.2979 (0.2844)	1.7585 (0.5709)	2.5108 (0.1835)
SMC	1.2590 (0.1606)	1.4655 (0.3043)	1.8590 (0.2030)
SWM	1.3279 (0.1255)	1.3099 (0.1187)	1.3939 (0.1356)
THL	1.3509 (0.1118)	1.4493 (0.1852)	1.6301 (0.2115)
VFC	1.2872 (0.2406)	1.6359 (0.4439)	2.2177 (0.1813)

4.4.3 Statistical Analyses

Partial least squares (PLS) analyses were performed based on region-of-interest and voxel-based functional image data (two slices), to produce summary scores. In addition, PLS analyses were also performed based on region-of-interest and voxel-based functional (two slices) imaging data by applying randomized singular value decomposition (PLS-RSVD) to determine if the results are similar to those of PLS analysis without applying RSVD. If the results are similar, we can conclude that the PLS-RSVD method is equivalent to PLS analysis using SVD, and we will apply it to a larger dataset. The dataset consisted of seventy-four CT, twenty-eight MCI and twenty AD subjects for the region-of-interest analyses and thirty-six CT, fifteen MCI and eleven AD subjects for the functional voxel-based analyses.

The PIB and FDG region-of-interest (or voxel-based functional image data) measures are each represented by a block and are referred to as X and Y, respectively. For the region-of-interest analyses, the elements of the blocks are numbered from X_1 to X_{17} and Y_1 to Y_{17}, each representing a specific region-of-interest for PIB and FDG. For two slices of the voxel-based

functional image data, the elements of the blocks are numbered from X_1 to X_{2970} and Y_1 to Y_{2970}, each representing a specific voxel (after applying an image masking) for two slices from the functional image data for PIB and FDG, respectively. For the voxel-based data for the whole brain, the elements of the blocks are numbered from X_1 to X_{42310} and Y_1 to Y_{42310}, each representing a specific voxel (after applying an image masking) in the functional image data for PIB and FDG, respectively. We therefore had a 17 by 17, 2970 by 2970 and 42310 by 42310 cross-correlation matrix for the region-of-interest, voxel-based (two slices), and voxel-based data for the whole brain, respectively. The elements of the cross-correlation matrix measure the correlation between a given region-of-interest (or voxel) for PIB and a given region-of-interest (or voxel) for FDG. PLS explains the cross-correlation matrix between PIB and FDG measures.

PLS analyses were also performed applying randomized singular value decomposition (RSVD) to approximate the singular value decomposition (SVD). RSVD was performed on the cross-correlation matrix of PIB by FDG (17 by 17 for region-of-interest, 2970 by 2970 for two slices of the voxel-based functional image data, and 42310 by 42310 for the voxel-based functional image data for the whole brain) to obtain PIB summary scores. RSVD was also performed on the cross-correlation matrix of FDG by PIB to obtain FDG summary scores. The number of rows sampled from the cross-correlation matrix for region-of-interest data was 5 and 10. For the functional image data (two slices), the number of rows sampled from the correlation matrix was 100, 500 and 1500. For the functional image data (whole brain, all slices), the number of rows sampled were 100 and 500. A resampling method (ten, twenty and thirty samples) was also applied to obtain a better estimate of the singular vectors, and therefore a better estimate of the summary scores. Kendall's coefficient of concordance, which is used to measure agreement between k orderings, was computed to test for agreement between the

summary scores. This measurement makes no assumptions regarding the nature of the probability distribution and can handle any number of distinct outcomes. The PLS and PLS-RSVD routines were programmed in R software (Bell Laboratories, Lucent Technologies, 2008).

4.4.4 Results

We applied PLS to explain the covariance in the cross-correlation matrix between PIB and FDG in terms of region-of-interest and functional imaging data.

PLS Region-of- interest Analysis

The singular value decomposition of the cross correlation matrix yielded seventeen pairs of latent variables and singular values. The singular values provide an index of the covariance between each of these pairs. The singular values for the first and second pair of latent variables were 0.1356 and 0.0144, respectively. The percentages of the variance explained by the first and second pairs of latent variables were 98.08% and 0.01%, respectively. Therefore, the first pair of latent variables is particularly important since it explained 98% of the summed squared cross-correlation. We examined the weights to understand the covariance between the first pair of latent variables. The weights within a latent variable A indicate which measurements are driving the covariance with the corresponding latent variable B. The FDG latent variables have 17 weights and the PIB latent variables have 17 weights. An assessment of the individual weights shows that LTC, PAC, PCL, PCM and SMC are most related (highest weights, greater than 0.30) to the first FDG ROI latent variable and DFC, PAC, PCM, PCU and SAC are most related to the first PIB ROI latent variable. Regions that are most related to the first PIB latent variable are consistent with results reported by Price et al. (2005) and Ziolko et al. (2006).

Summary scores for FDG and PIB were also calculated for each subject and are shown in Figures 3 and 4. The FDG summary scores resulted in lower numbers when compared to the PIB summary scores. The PIB summary scores show a clear clustering of scores between AD and CT subjects with the exception of one subject. The assessment of this outlier reveals that ROI measurements for this subject were similar to those of the AD subjects. The FDG summary scores do not show any clustering between the groups. The summary scores for MCI subjects, for both FDG and PIB, fall within the range of both Alzheimer's disease and control subject scores. The summary scores were also plotted against the MMSE scores (Figure 5 and 6). These results also show a clear separation between AD and control subjects for PIB data. Figure 7 shows that there is an inverse relationship between PIB and FDG.

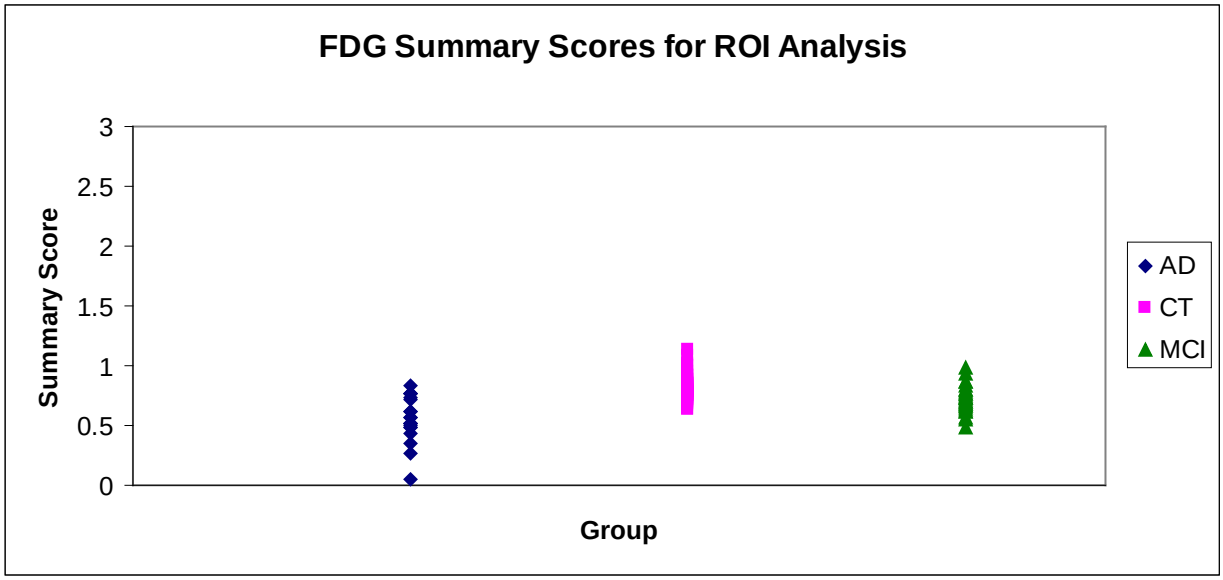

Figure 3 FDG PET Summary Scores for ROI analysis

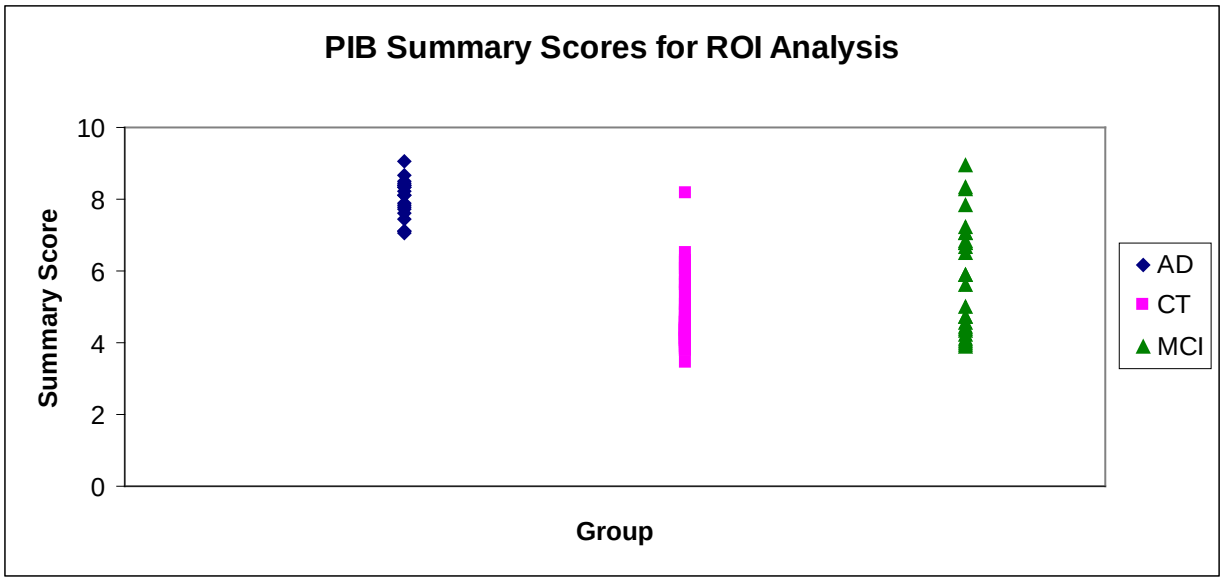

Figure 4 PIB PET Summary Scores for ROI analysis

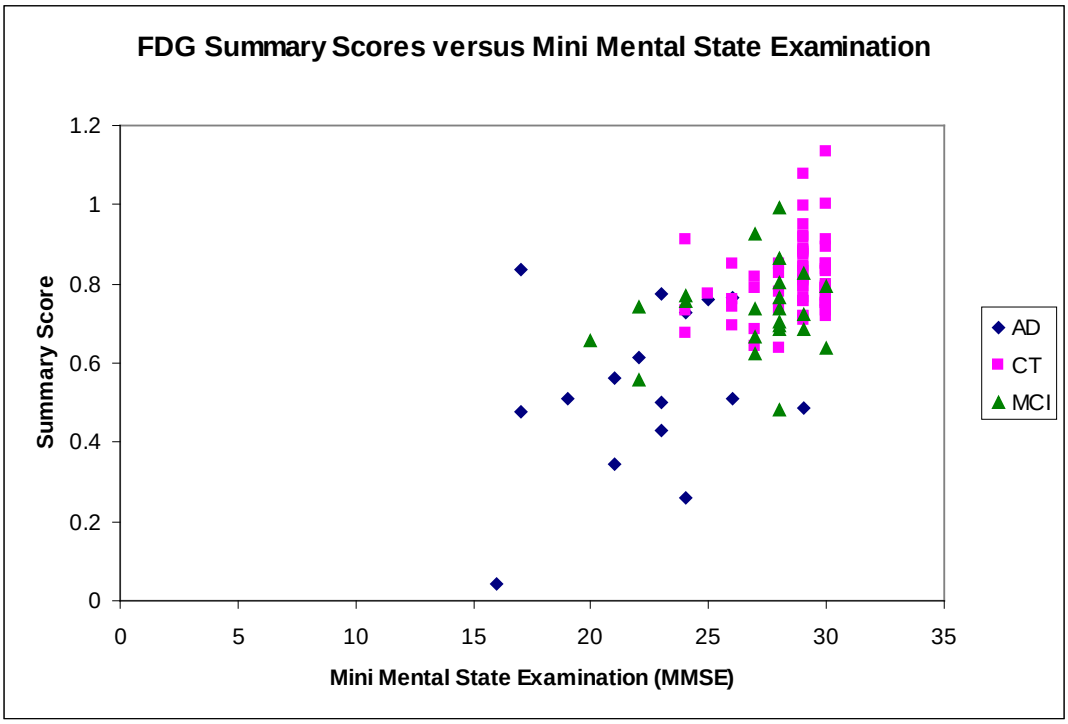

Figure 5 PLS results for FDG plotted by Mini Mental State Examination (MMSE) for ROI analysis

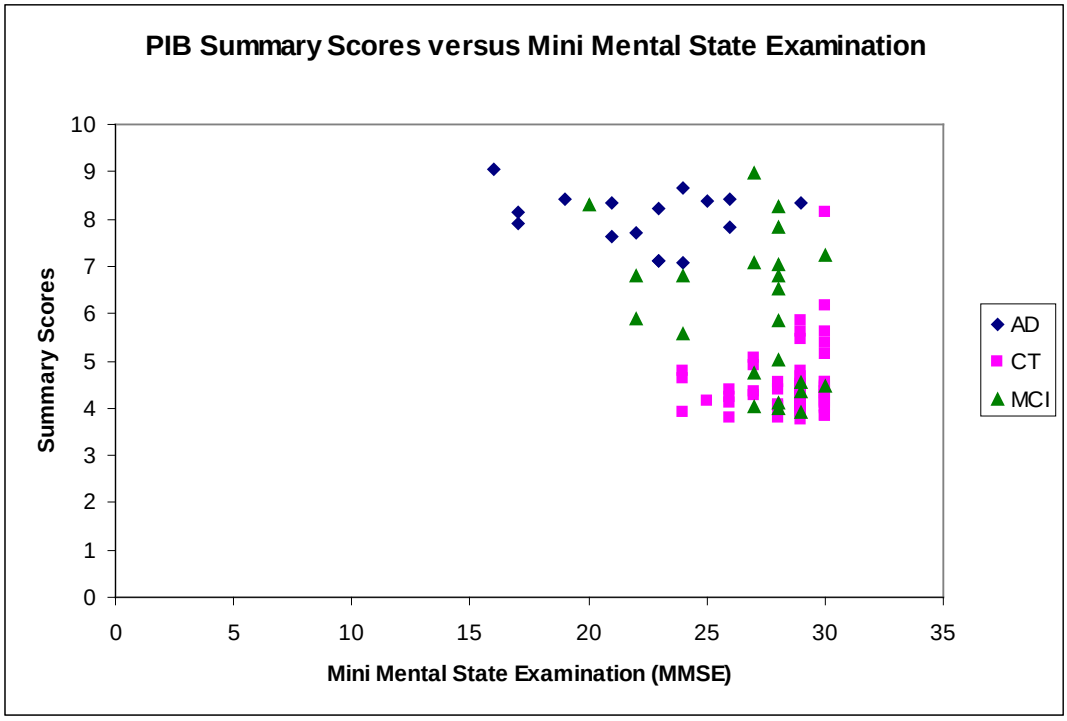

Figure 6 PLS results for PIB plotted by Mini Mental State Examination (MMSE) for ROI analysis

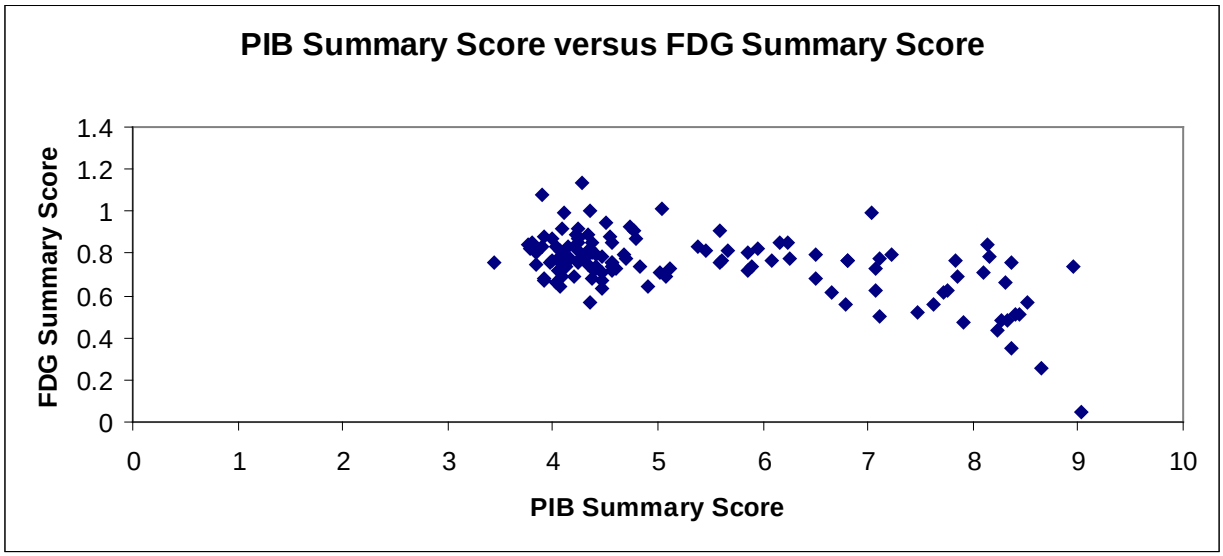

Figure 7 PIB Summary Scores versus FDG Summary Scores for ROI Analysis

RSVD Application for PLS Region-of- interest Analysis

The PLS analyses applying RSVD with 5 and 10 rows sampled (10, 20 and 30 samples) showed similar summary score results when compared to the PLS analysis computed from the full matrix (Figures 8-12). Even though the approximation was slightly underestimated (or overestimated), the resulting pattern remained the same. Kendall's coefficient of concordance results showed that there is agreement among the scores with respect to how they are calculated (p <0.001). That is, there is agreement between the scores obtained from PLS and the scores obtained from PLS-RSVD analyses. Therefore, we only focus on example results for 10 rows and 10 samples.

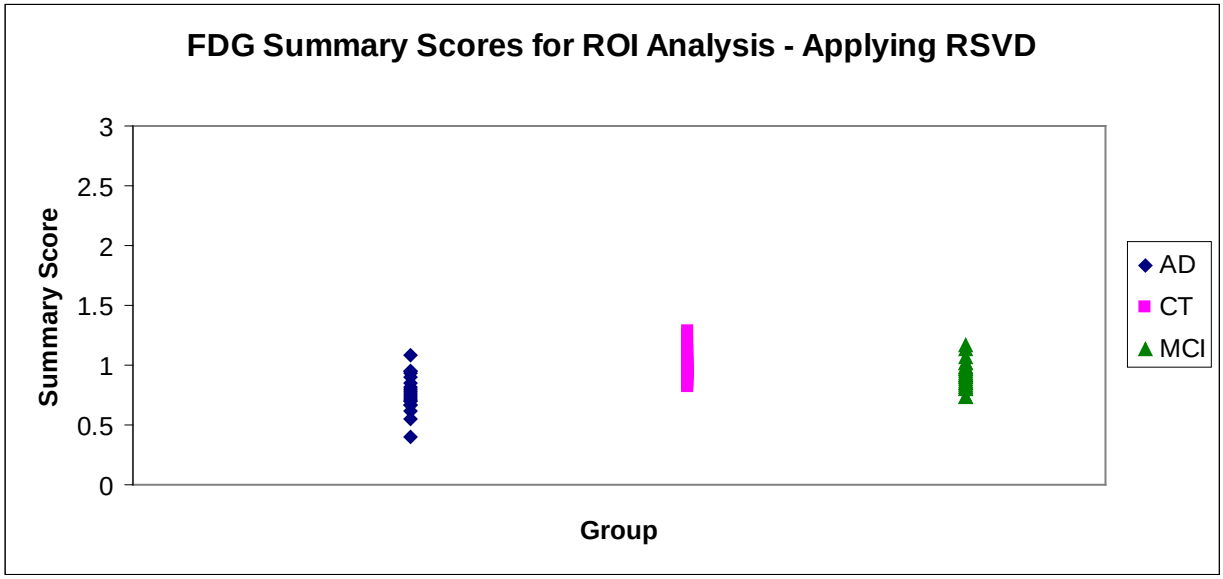

Figure 8 Summary Scores for FDG PET for ROI analysis when applying RSVD

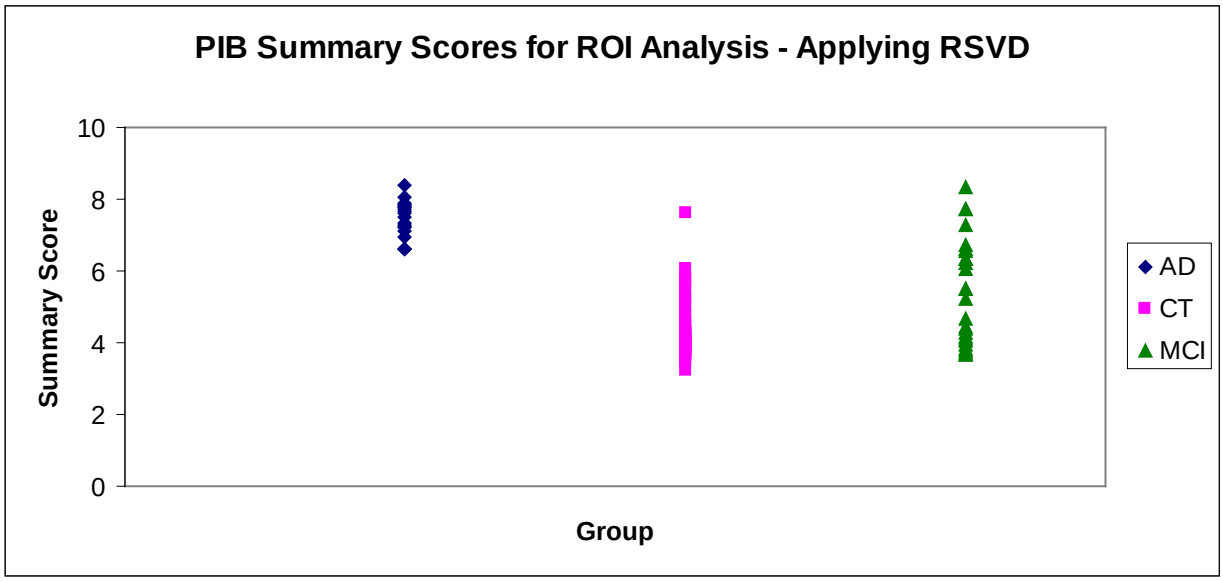

Figure 9 Summary Scores for PIB PET for ROI analysis when applying RSVD

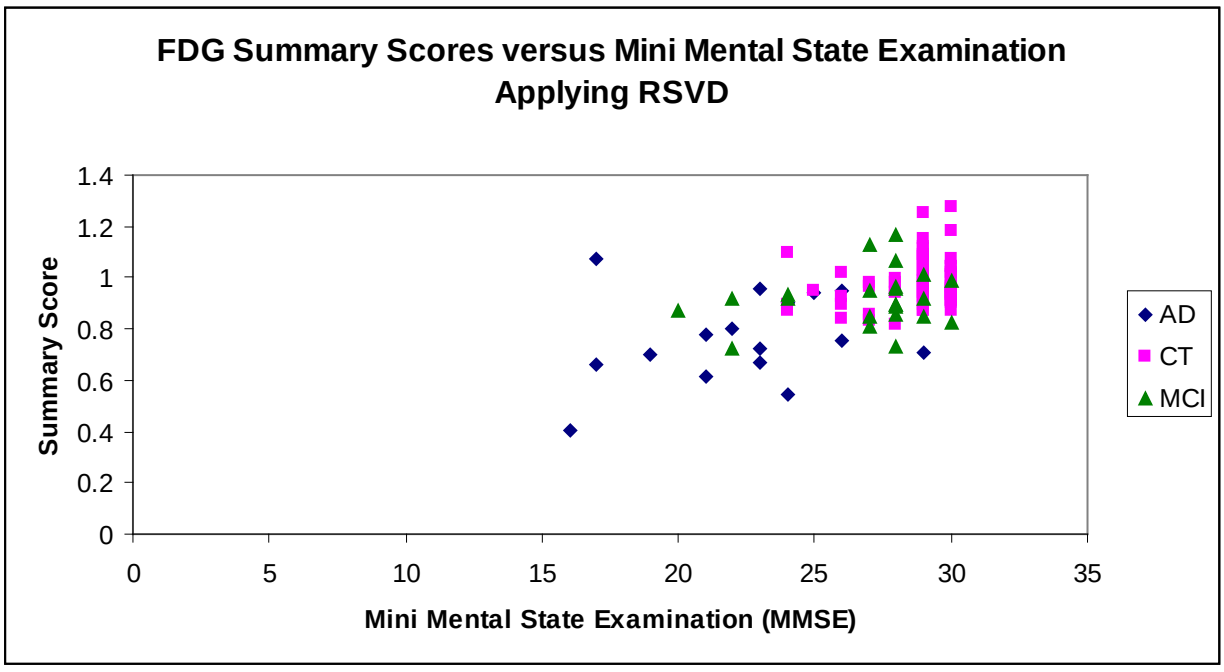

Figure 10 PLS results for FDG plotted by Mini Mental State Examination (MMSE) for ROI analysis when applying RSVD

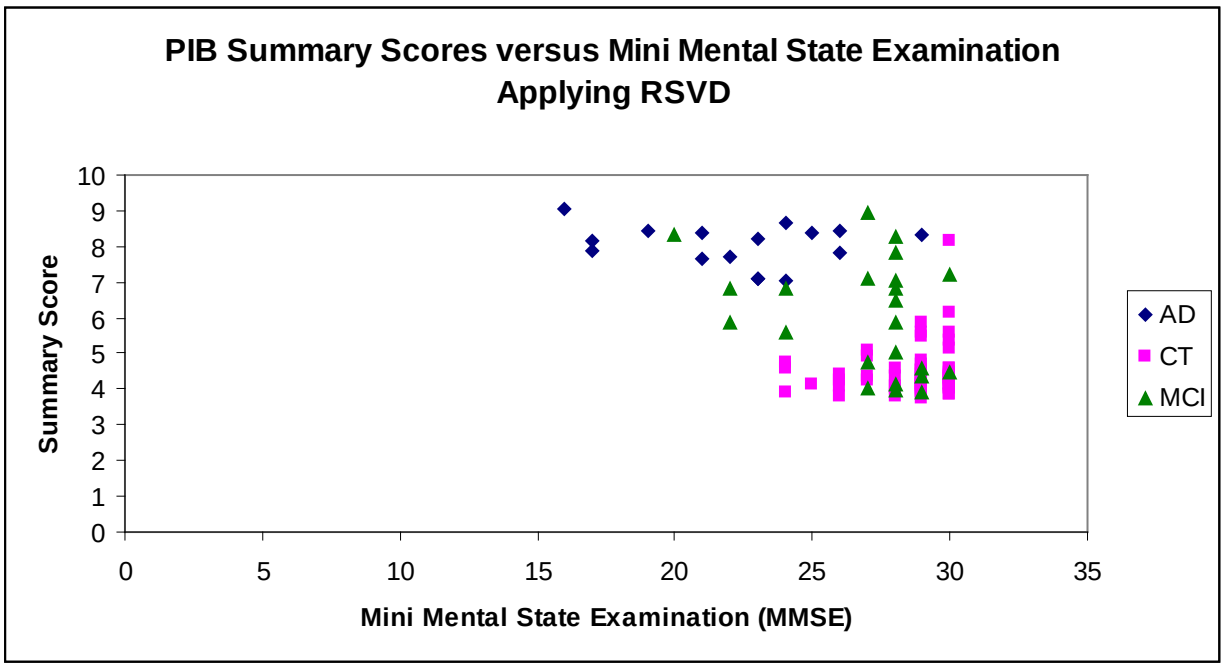

Figure 11 PLS results for PIB plotted by Mini Mental State Examination (MMSE) for ROI analysis when applying RSVD

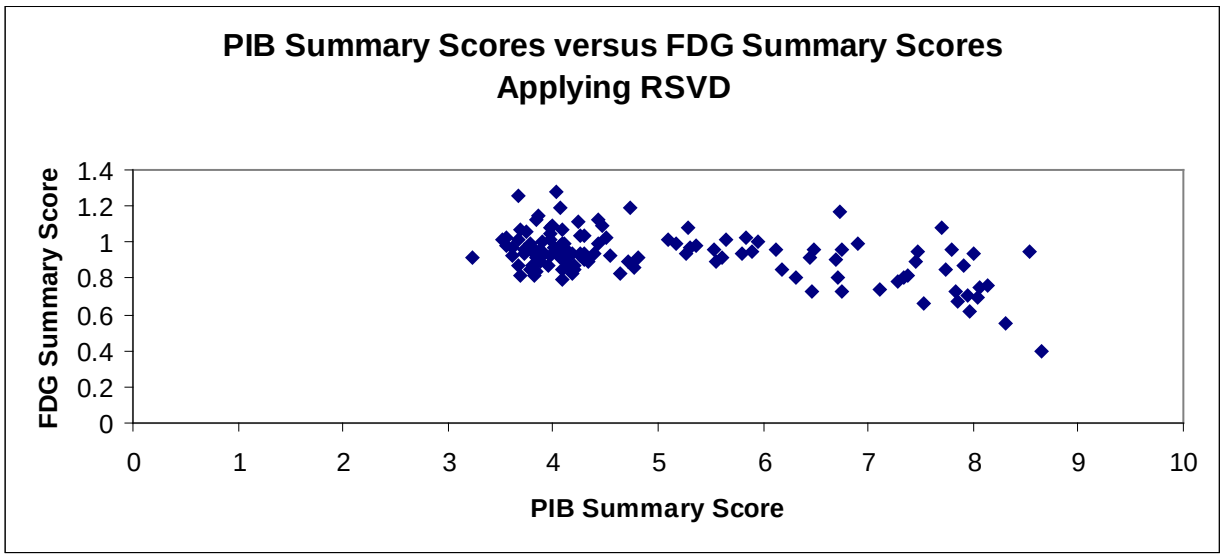

Figure 12 PIB Summary Scores versus FDG Summary Scores for ROI Analysis when applying RSVD

PLS Voxel-based Analysis - Two Slices from functional image data

The singular value decomposition of the cross correlation matrix yielded 2970 pairs of latent variables and singular values. The singular values for the first and second pair of latent variables were 17.9416 and 3.8150 accounting for 87.33% and 3.95% of the summed squared cross-block correlation, respectively. Therefore, the first pair of latent variables explained approximately 87% of the variation. Results for only the first pair of latent variable are described below.

Summary scores for FDG and PIB were calculated for each subject and are shown in Figures 13 and 14, respectively. The FDG summary scores resulted in a smaller range of values when compared to the PIB summary scores. The PIB summary scores show a clear clustering of scores between AD and CT subjects. In contrast, the FDG summary scores do not show any distinction between the groups. The summary scores for MCI subjects, for both FDG and PIB, fall within the range of both Alzheimer's disease and control subjects scores. The summary scores were also plotted against the MMSE scores (Figure 15 and 16). These results also show a clear separation between AD and control subjects for the PIB data. Figure 17 shows a comparison of the FDG and PIB summary scores for each subject. Even though the FDG summary scores were lower than the PIB summary scores, the PIB scores indicate more variability when compared to the FDG scores. When comparing the PIB and FDG summary scores, results show that there is an inverse relationship (Figure 18).

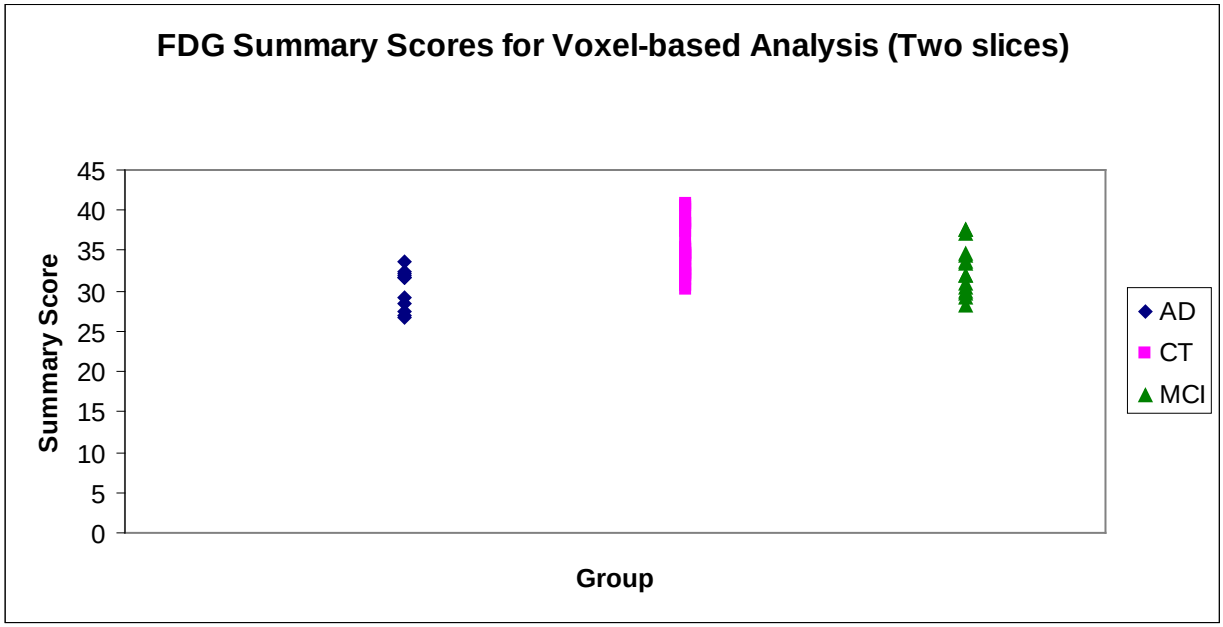

Figure 13 Summary Scores for FDG for voxel-based analysis (two slices) from functional image data

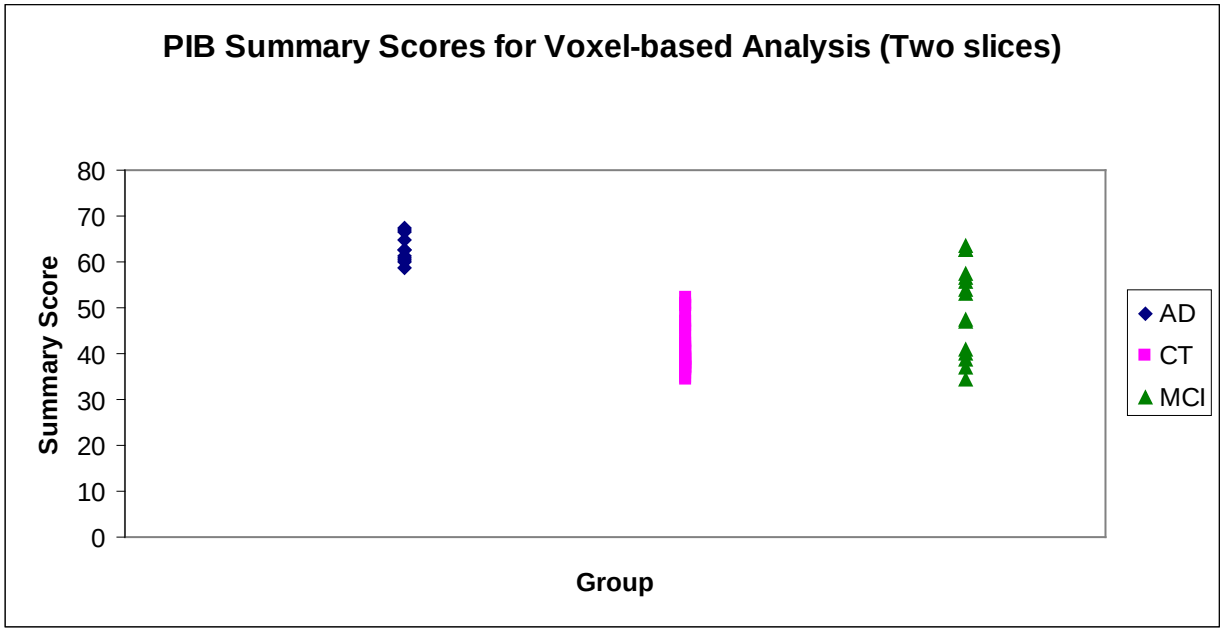

Figure 14 Summary Scores for PIB for voxel-based analysis (two slices) from functional image data

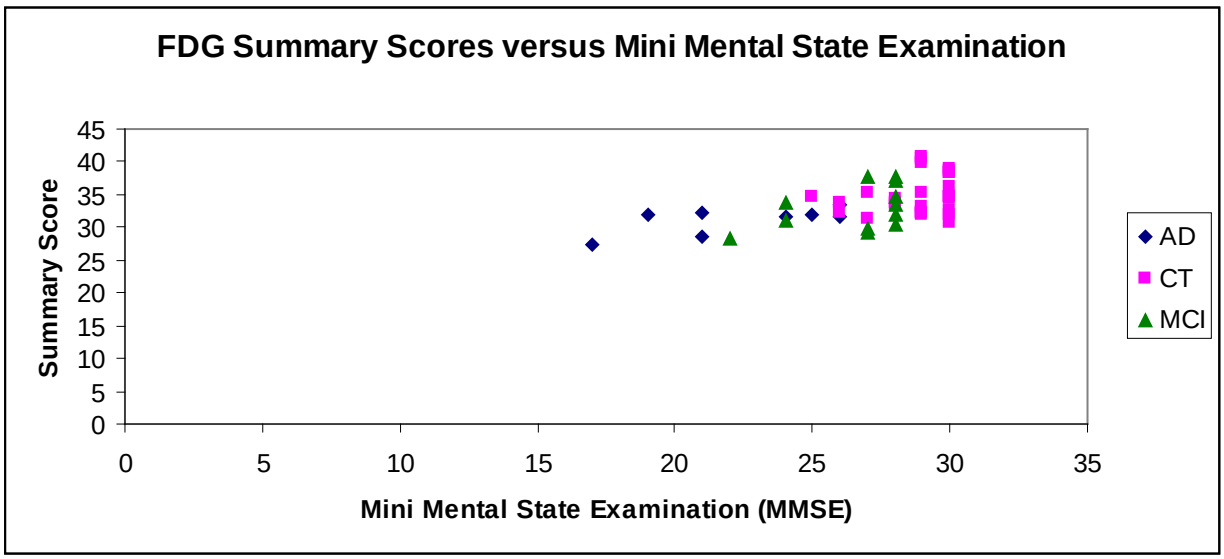

Figure 15 PLS results for FDG plotted by Mini Mental State Examination (MMSE) for voxel-based analysis (two slices) from functional image data

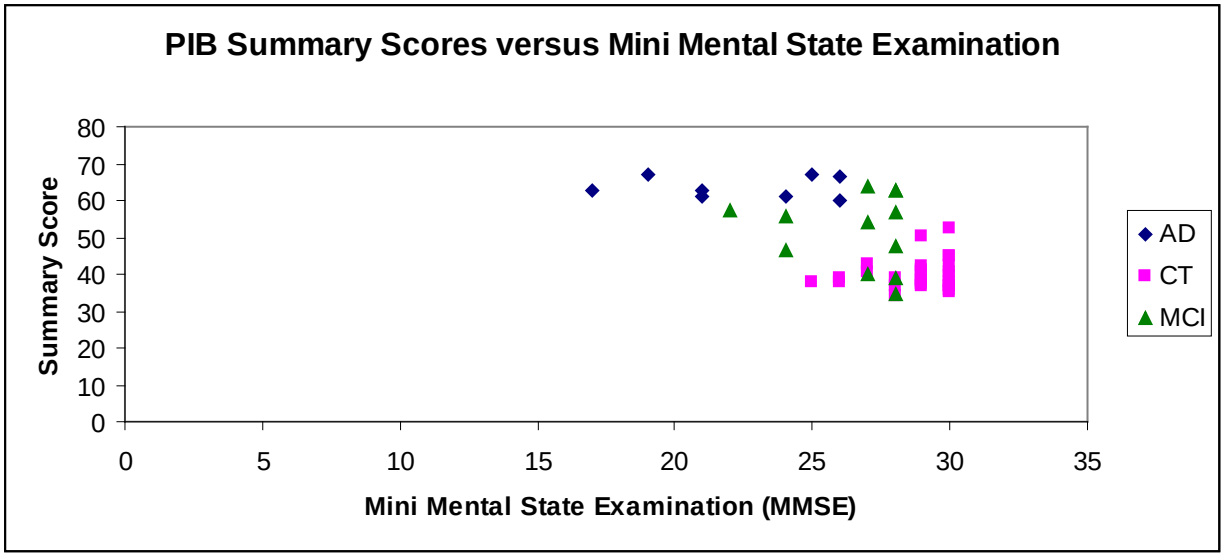

Figure 16 PLS results for PIB plotted by Mini Mental State Examination (MMSE) for voxel-based analysis (two slices) from functional image data

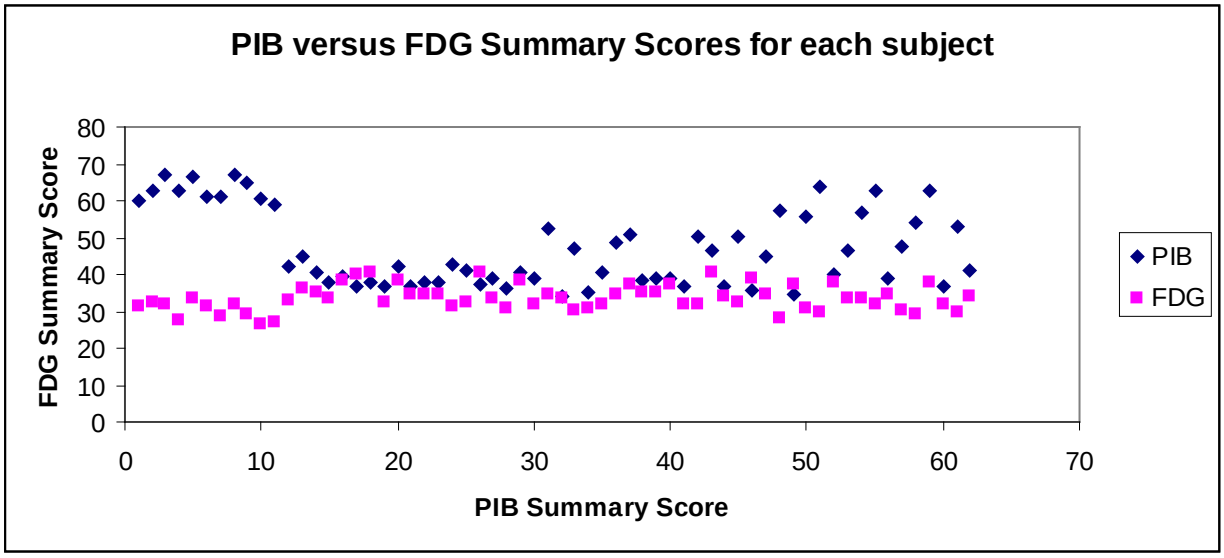

Figure 17 Summary Scores for PIB and FDG for each subject for voxel-based data (two slices) from functional image data

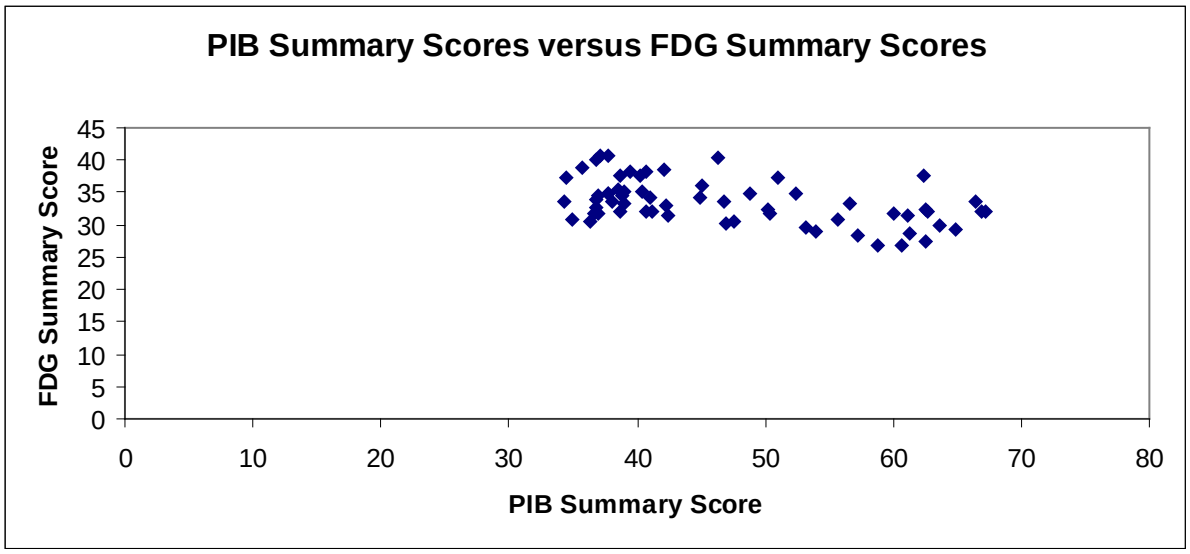

Figure 18 PIB Summary Scores versus FDG Summary Scores for voxel-based data (two slices) from functional image data

RSVD Application for PLS Voxel-based Analysis – Two Slices from functional image data

The PLS analyses applying RSVD with 100 rows, 500 rows and 1500 rows sampled (10, 20 and 30 samples) showed similar summary score results when compared to the PLS analysis computed from the full matrix (Figures 19-24). Even though the approximation was slightly underestimated (or overestimated), the resulting pattern remained the same. Kendall's coefficient of concordance results showed that there is agreement among the scores with respect to how they are calculated (p <0.001). That is, there is agreement between the scores obtained from PLS and the scores obtained from PLS-RSVD analyses for functional image data (two slices). Therefore, we only focus on example results for 1500 rows and 10 samples. The PIB summary scores show clear separation between the Alzheimer's disease and control groups. The summary scores for MCI subjects, for both FDG and PIB, fall within the range of both Alzheimer's disease and control subject scores.

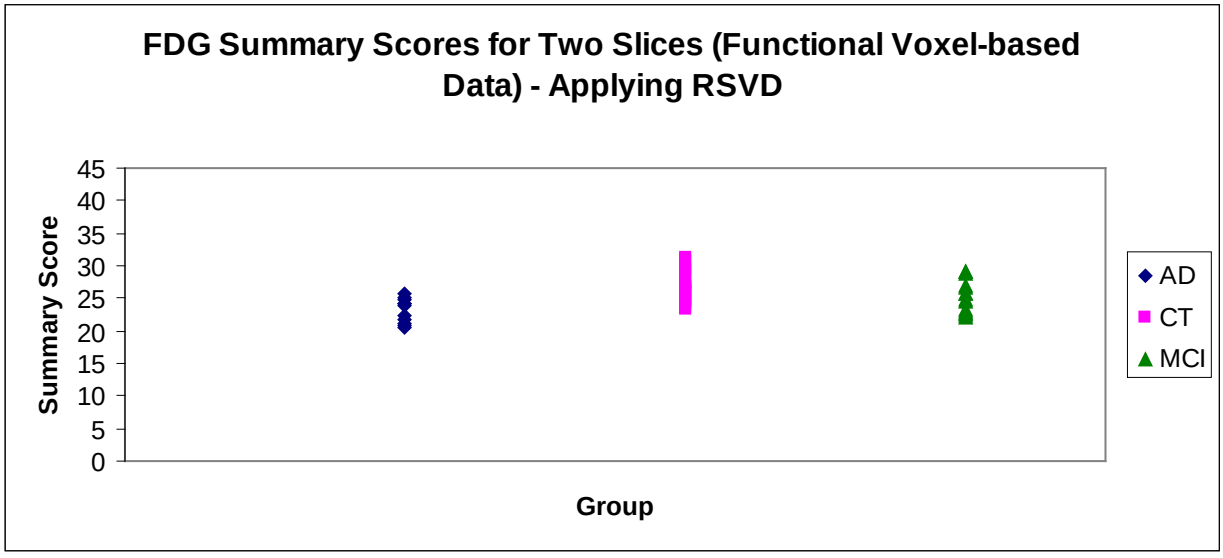

Figure 19 Summary Scores for FDG for voxel-based functional data (two slices) when applying RSVD

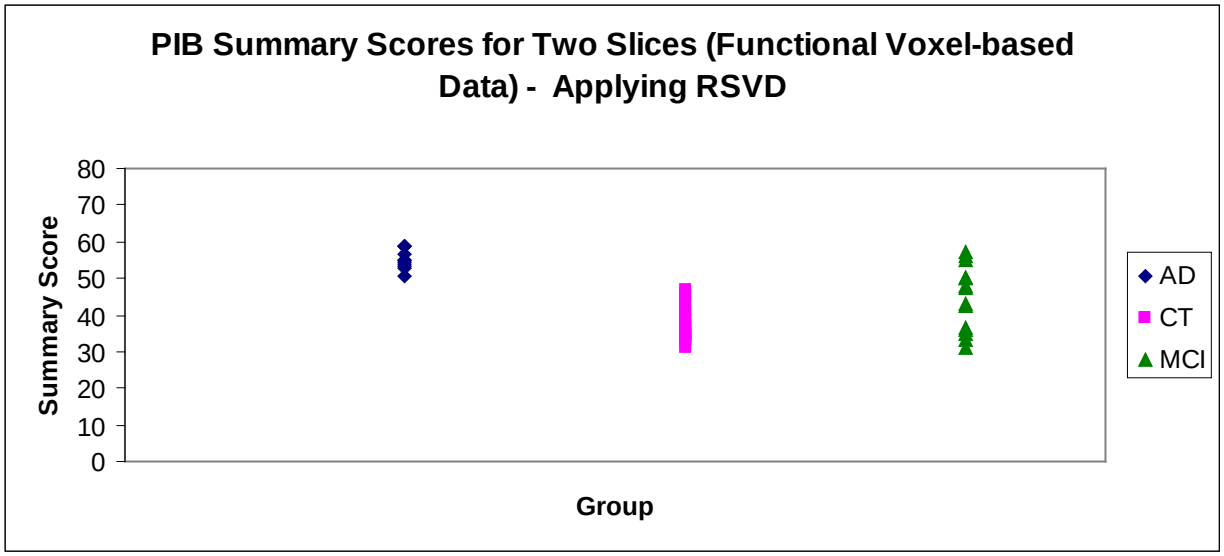

Figure 20 Summary Scores for PIB for voxel-based functional data (two slices) when applying RSVD

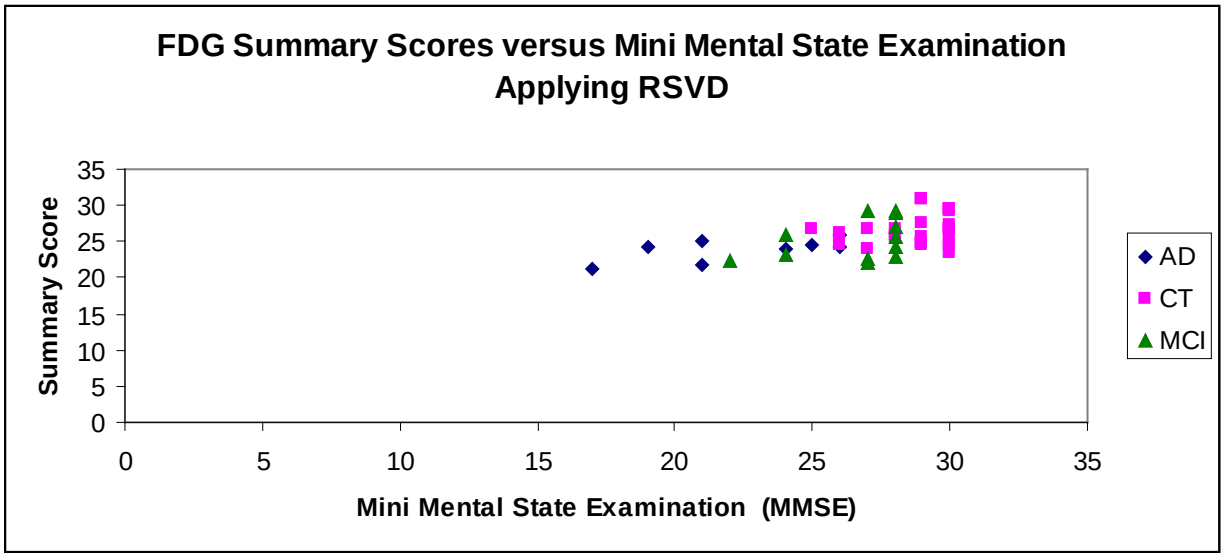

Figure 21 PLS results for FDG plotted by Mini Mental State Examination (MMSE) for voxel-based functional image data (two slices) when applying RSVD

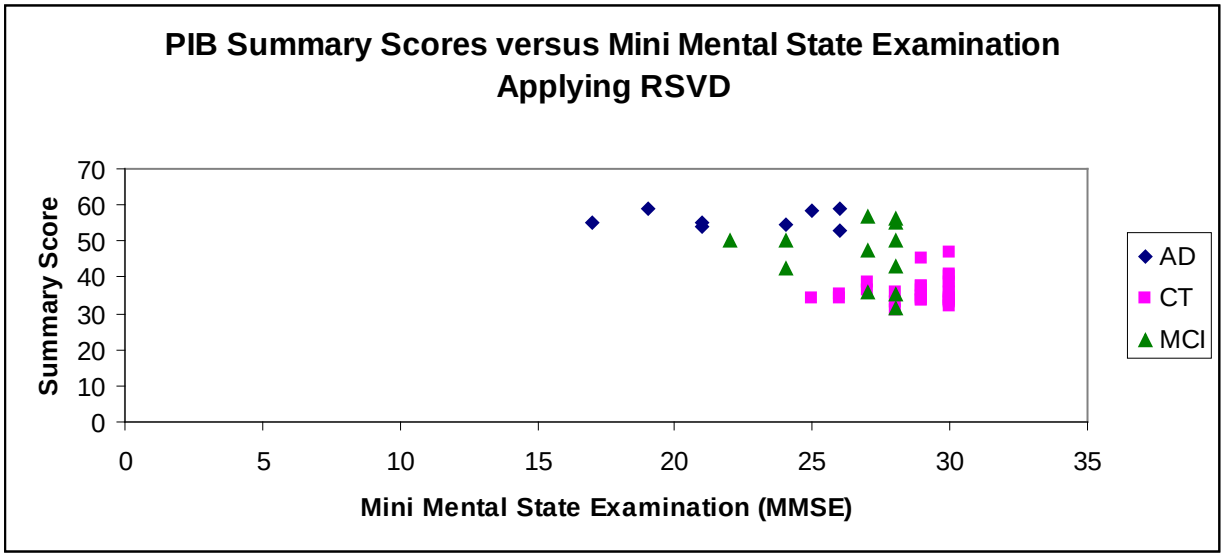

Figure 22 PLS results for PIB plotted by Mini Mental State Examination (MMSE) for voxel-based functional image data (two slices) when applying RSVD

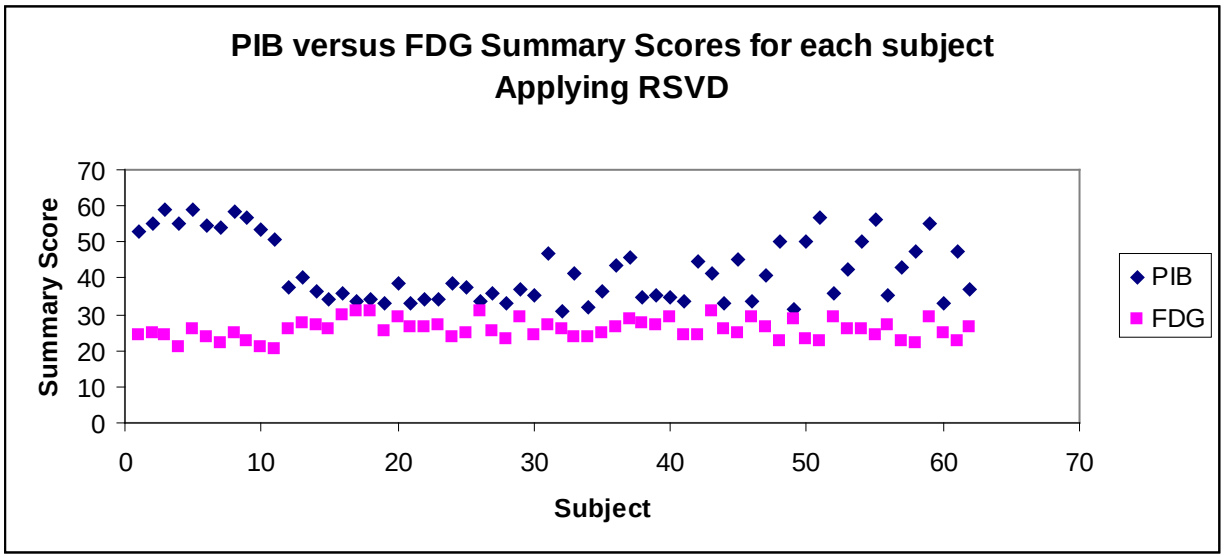

Figure 23 Summary Scores for PIB and FDG for each subject for voxel-based functional image data (two slices) when applying RSVD

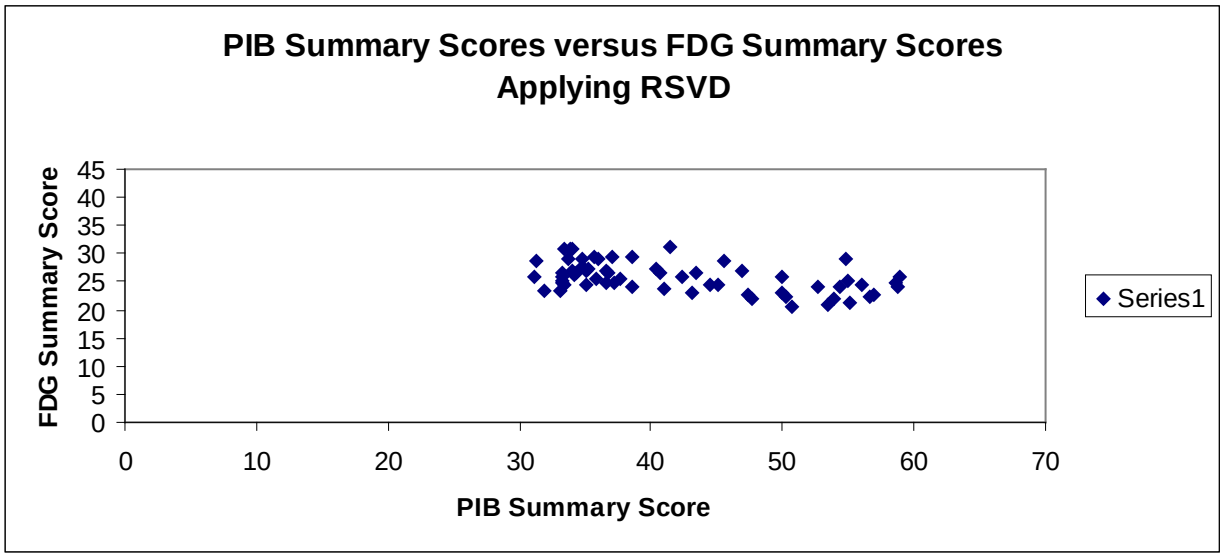

Figure 24 PIB Summary Scores versus FDG Summary Scores for voxel-based data functional image data (two slices) when applying RSVD

RSVD Application for PLS Voxel-based Analysis – Functional image data for the whole brain

Given that the results from the PLS analyses and PLS-RSVD analyses were similar for both datasets (ROIs and voxel-based data (two slices)) we can conclude that RSVD provides a good approximation of the singular vectors and therefore good approximation of the summary scores. Therefore, PLS analysis was also performed by applying RSVD to the voxel-based functional image data for the whole brain. The RSVD was performed with 100 and 500 rows sampled (10, 20 and 30 samples). The singular values for the first and second pair of latent variables were approximately 263.6602 and 129.9172 accounting for 62.99% and 15.26% of the summed squared cross-block correlation, respectively. Therefore, the first and second pair of latent variables explained approximately 78.26% of the variation. Results for these two pairs of latent variable are described below.

Summary scores for FDG and PIB for both pairs of latent variables were calculated for each subject and are shown in Figures 25-28. The FDG summary scores resulted in a similar range of numbers when compared to PIB summary scores. The PIB summary scores, for the first and second latent variable, show a clear clustering of scores between AD and CT subjects. In contrast, the FDG summary scores (for both latent variables) do not show any distinction between the groups. The summary scores for MCI subjects, for both FDG and PIB, fall within the range of both Alzheimer's disease and control subject scores. The summary scores for the first pair of latent variables were also plotted against the MMSE scores (Figures 29-30). These results show a clear separation between AD and control subjects for the PIB data. Results for the second latent variable were similar (Results not shown). When comparing PIB and FDG summary scores, for the first and second latent variable, results show that, there is an inverse relationship (Figures 31-32).

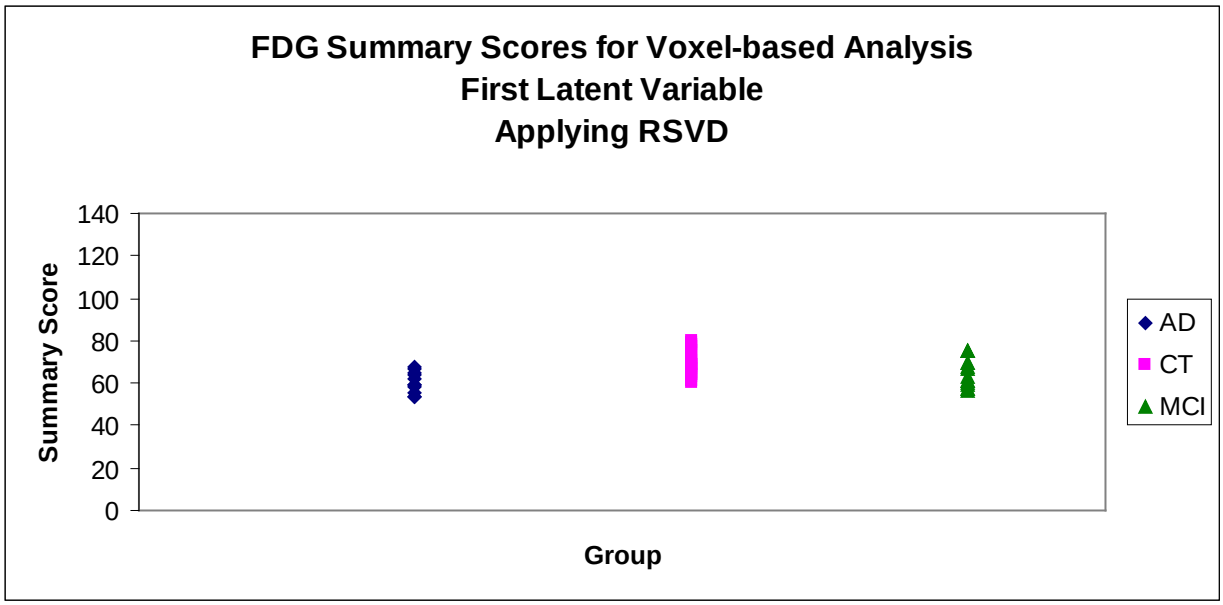

Figure 25 Summary Scores for FDG (first latent variable) for voxel-based functional image data for the whole brain when applying RSVD

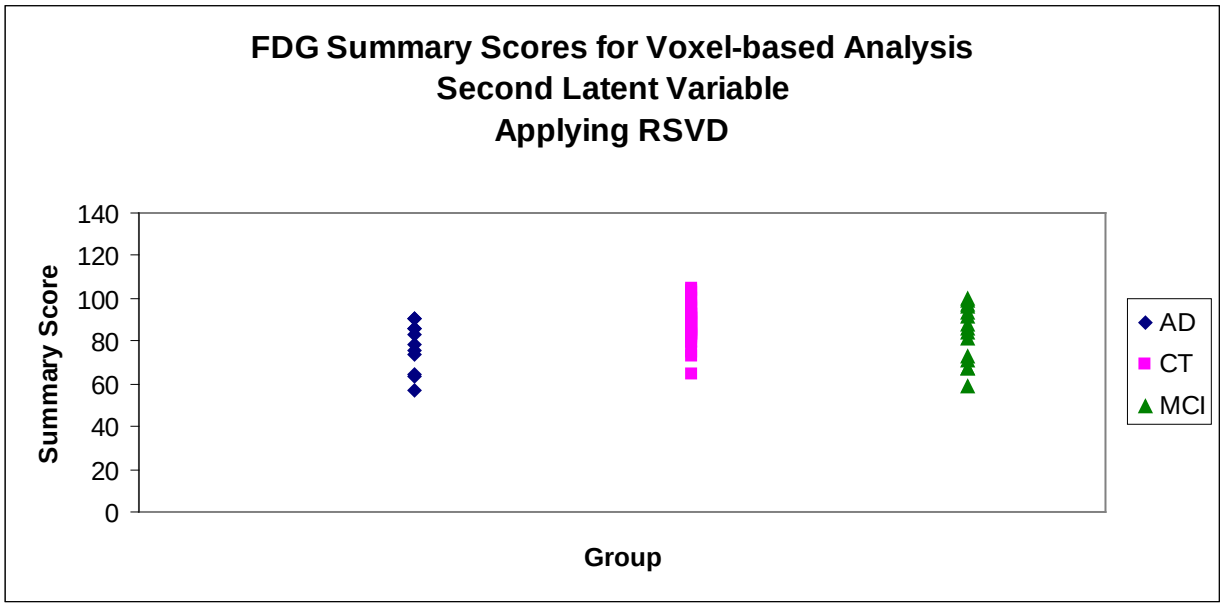

Figure 26 Summary Scores for FDG (second latent variable) for voxel-based functional image data for the whole brain when applying RSVD

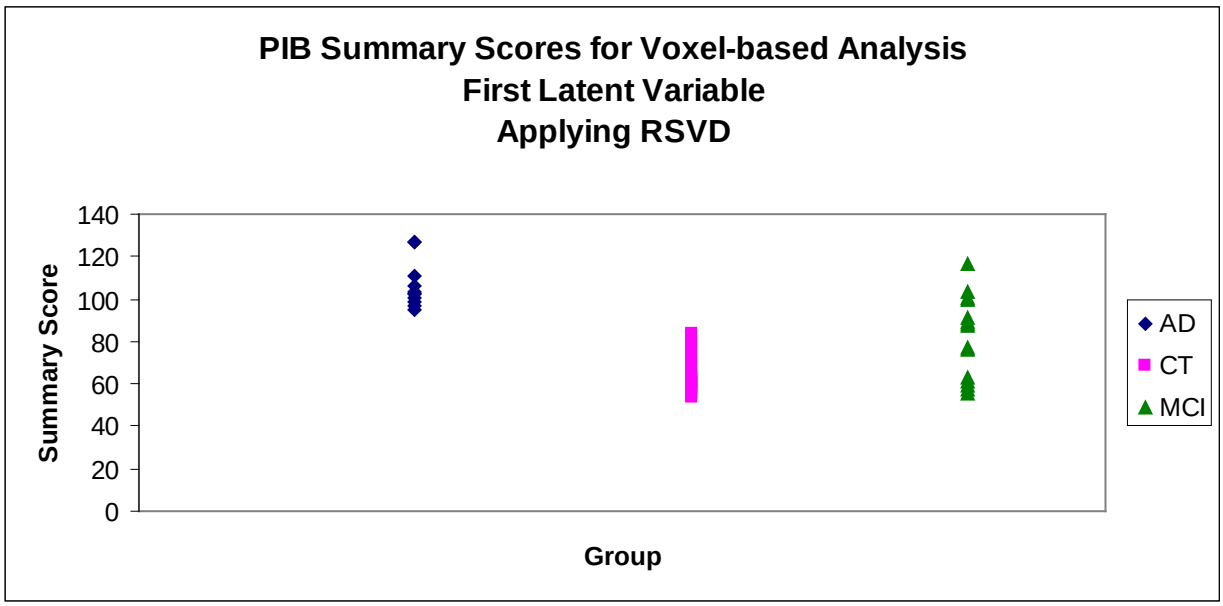

Figure 27 Summary Scores for PIB (first latent variable) for voxel-based functional image data for the whole brain when applying RSVD

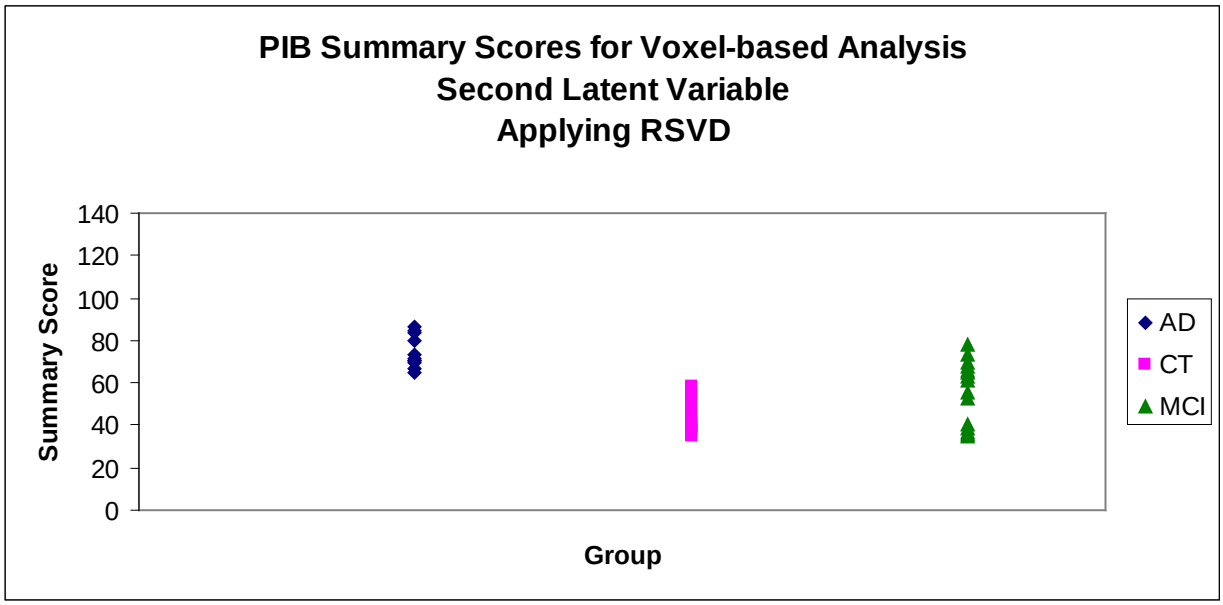

Figure 28 Summary Scores for PIB (second latent variable) for voxel-based functional image data for the whole brain when applying RSVD

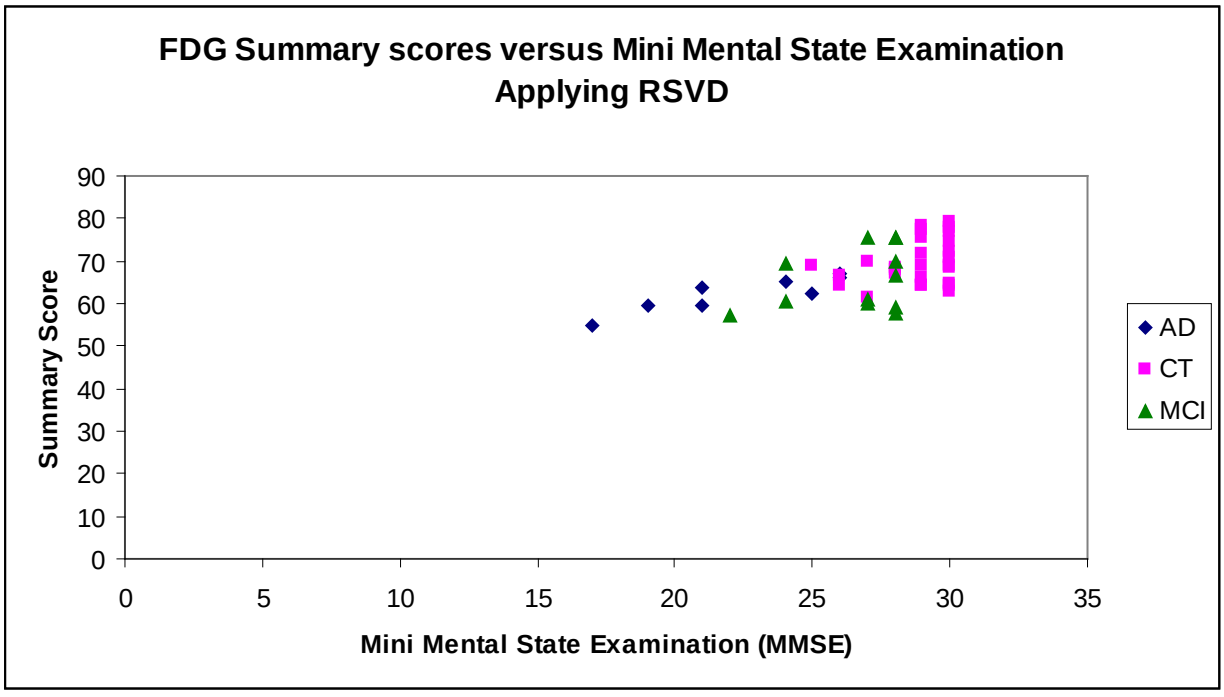

Figure 29 PLS results for FDG plotted by Mini Mental State Examination (MMSE) for voxel-based functional image data for the whole brain when applying RSVD

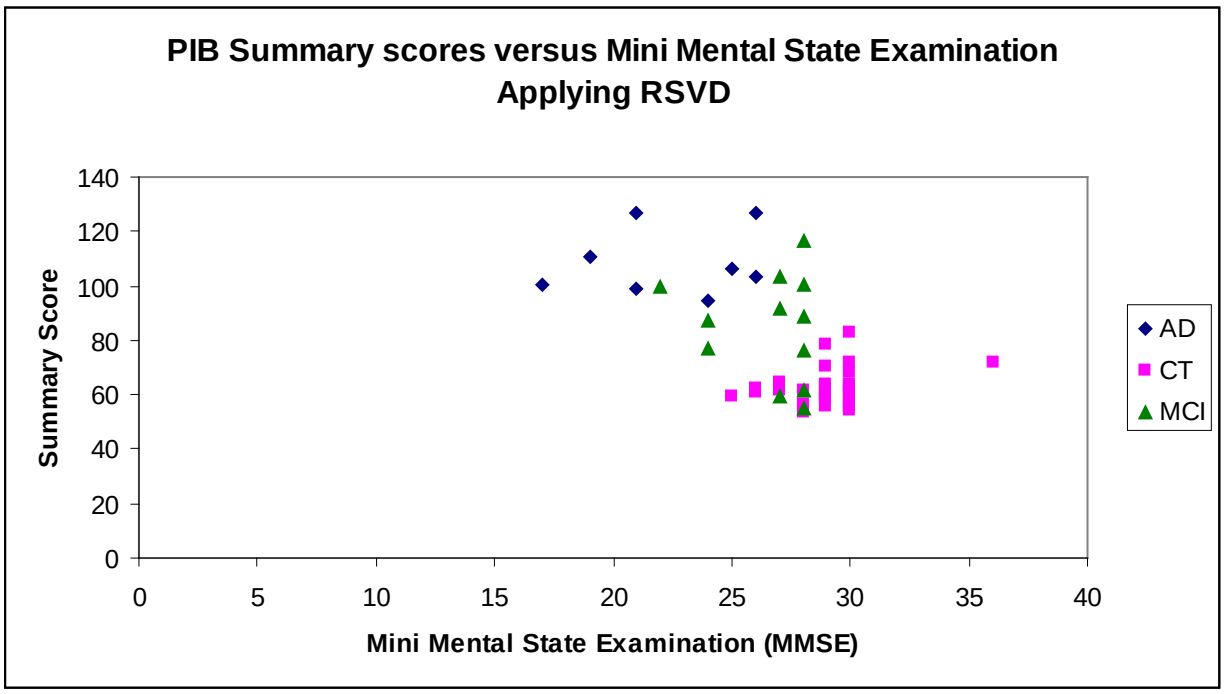

Figure 30 PLS results for PIB plotted by Mini Mental State Examination (MMSE) for voxel-based functional image data for the whole brain when applying RSVD

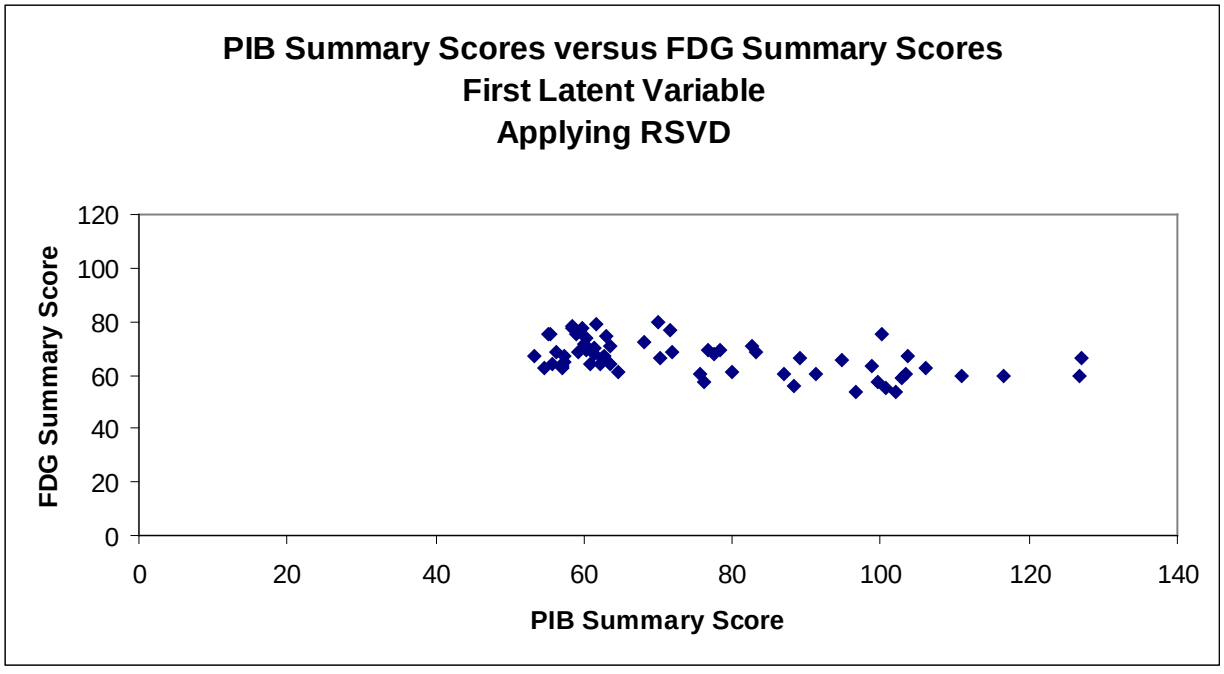

Figure 31 PIB Summary Scores versus FDG Summary Scores (first latent variable) for voxel-based functional image data for the whole brain when applying RSVD

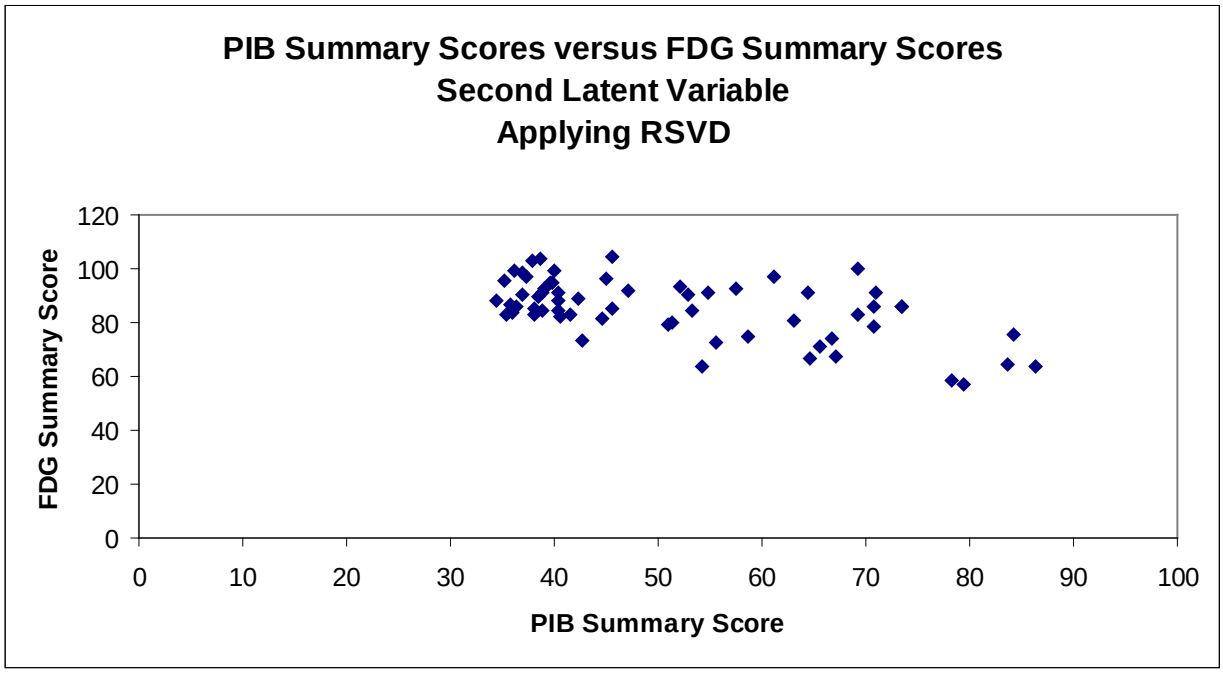

Figure 32 PIB Summary Scores versus FDG Summary Scores (second latent variable) for voxel-based functional image data for the whole brain when applying RSVD

4.5 CONCLUSIONS AND DISCUSSION

Previous studies have shown that FDG and PIB can assist with the diagnosis of Alzheimer's disease. Therefore, it is important to understand their relationship as they provide information about the disease process. The current work applies PLS to identify the relationship between FDG and PIB in terms of voxel-based functional data in a sample of seventy-four control, twenty-eight mild cognitive impairment and twenty Alzheimer's disease subjects. In addition, the current work was performed to evaluate PLS as a multivariate tool for the assessment of group differences for FDG and PIB. Results presented in this work have shown that PLS is an

effective multivariate analytic method for multimodality functional image data. The PLS results also show that there is an inverse relationship between FDG and PIB for both ROI and voxel-based analyses. In addition, PLS results show that the radioactive tracer PIB can be used to discriminate between AD and control subjects. In this study, we also applied a randomized singular value decomposition as an approximation technique for the computation of the SVD of a matrix, and therefore approximation of summary scores obtained from PLS analysis. The results showed that RSVD provides a good approximation of the singular vectors of a matrix, and therefore a good approximation of summary scores. This finding is relevant for high-dimensional setting applications (e.g. neuroimaging and microarray data) that require the computation of singular value decomposition of a large matrix that cannot be computed due to memory limitations, allowing the ability to overcome this limitation. Future work will include application of PLS and PLS-RSVD for the analysis of longitudinal data in neuroimaging and also developing a method to obtain better estimates of the singular vectors of a matrix by combining the RSVD method with updating the SVD of a matrix by a row deletion method.

5.0 ASSESSMENT OF PARAMETER SETTINGS FOR SPM5 SPATIAL NORMALIZATION OF STRUCTURAL MRI DATA: APPLICATION TO TYPE 2 DIABETES

Spatial normalization is the process of standardizing images of different subjects into the same anatomical space. The most widely used software to perform this process is Statistical Parametric Mapping (SPM). SPM is a tool designed for processing and analyzing brain imaging data. The primary goal of SPM analysis is to produce a meaningful statistical comparison between image sets. SPM consists of several components including realignment, co registration, spatial normalization, spatial smoothing, voxel-wise statistical analysis and segmentation that can be applied to imaging data. Spatial normalization is a critical pre-processing step in the analysis of brain imaging data since it produces the "raw" data the subsequent analyses. Therefore, it is important to study and understand how spatial normalization in SPM works under different conditions and parameter settings.

The standard normalization method in SPM5 minimizes the sum of squared differences between the subject's image and the template, while maximizing the prior probability of the transformation. Spatial normalization begins by determining the optimum twelve-parameter affine transformation to account for differences in position, orientation and overall brain size. After affine transformation, a nonlinear transformation is applied to correct for gross differences in head shape that were not accounted by the affine transformation. The nonlinear deformations

are described by the lowest frequency components of three-dimensional discrete cosine transform basis functions (Ashburner and Friston, 1999). For the standard method, the user has the ability to select parameter estimate settings for the nonlinear transformation.

The unified method combines segmentation, spatial normalization and bias correction in a unified model approach (Ashburner and Friston, 2005). Spatial normalization begins with an affine transformation to achieve an approximate alignment. Then, deformation of the tissue probability maps is performed to achieve a better model fit to the data. Similar to the standard method, the unified model option allows the user to choose different values of the warp frequency cutoff and warping regularization.

This chapter presents a study published in the journal NeuroImage (Rosario et al., 2008). The published paper, included in Appendix A, assesses the effect of different parameter settings for spatial normalization, standard and unified methods, in SPM5. Results from this study showed that changes in the parameter settings in SPM5 affect the performance of the spatial normalization when applying the standard method. However, when the unified method was applied, changes in the parameter settings did not affect the performance of the normalization.

6.0 THIN PLATE SPLINES FOR NONLINEAR TRANSFORMATION OF MAGNETIC RESONANCE IMAGING

6.1 INTRODUCTION AND PROBLEM DESCRIPTION

The comparison of structural or functional brain images of different subjects requires the reduction of inter-individual variability. Spatial normalization is an image processing technique that can remove this variability. This technique is the process of applying a spatial transformation that moves and warps images from a number of subjects so that they map onto the same coordinate system or standard anatomical space defined by a template. That is, the objective of normalization is to remove unwanted differences between the subjects' images to allow subsequent analysis of the data. Spatial normalization typically involves rotations and translation, and nonlinear warping of the brain to match a standard template. Image warping is an essential imaging pre-processing step for voxel-based analyses of brain data because it produces the "raw" data for subsequent statistical analyses. This step ensures that data from different subjects are derived from homologous regions in the brain.

Several methods are available to perform spatial normalization of images. These methods include Statistical Parametric Mapping (SPM), Automated Image Registration (AIR), Analysis of Functional NeuroImages (AFNI), Spatial Normalization (SN), and NEUROSTAT, among others. The most widely used software for spatial normalization in research literature is

SPM. As explained in the previous chapter, the standard normalization method in SPM5 minimizes the sum of squared differences between the subject's image and the template, while maximizing the prior probability of the transformation. Spatial normalization begins by determining the optimum twelve-parameter affine transformation to account for differences in position, orientation and overall brain size. After affine transformation, a nonlinear transformation is applied to correct for gross differences in head shape that were not accounted for by the affine transformation. The nonlinear deformations are described by the lowest frequency components of three-dimensional discrete cosine transform basis functions (Ashburner and Friston, 1999). The user has the ability to select different parameter estimate settings for nonlinear transformation such as nonlinear frequency cutoff, nonlinear regularization and the number of nonlinear iterations. The unified method combines segmentation, spatial normalization and bias correction in a unified model approach (Ashburner and Friston, 2005). Spatial normalization begins with an affine transformation to achieve an approximate alignment. Then, deformation of the tissue probability maps is performed to achieve a better model fit to the data. Similar to the standard method, the unified model option allows the user to select different values of the warp frequency cutoff and warping regularization.

Normalization methods can be grouped into two categories: intensity-based or label-based. The intensity-based approach uses voxel similarity measures between the source and reference image, such as squared sum of intensity differences or normalized cross-correlation. On the contrary, the label-based approach identifies homologous features, such as points, lines or surfaces, in the source and reference image and finds the transformation that best superpose them. In this work, we focus on a point-based approach for spatial normalization and apply thin

plate spline methods for linear and nonlinear transformation of three-dimensional magnetic resonance imaging.

The thin plate spline (TPS) is an effective tool for modeling coordinate transformations. A TPS interpolation maps a point from a reference image to the corresponding point in the target image. The use of TPS in image warping involves minimizing the bending energy function of a transformation over a set of landmark points. The TPS model has several advantages: (1) the model has closed form solution (2) it has no free parameters that need manual tuning by the user and (3) the interpolation is smooth with derivatives of any order and (4) this method can be significantly faster than other spatial normalization methods that are already available. On the other hand, a drawback of this tool is that it requires the solution of a linear system of equations whose size increases with the number of landmark points and can be computationally expensive when used on large datasets. We applied a three-dimensional thin plate spline interpolation model for image warping of magnetic resonance imaging. In addition, we applied a smoothing thin plate spline to account for landmark localization errors. This chapter is organized as follows: first, we present the interpolation thin plate spline method and then we describe the extension to an approximation method (smoothing thin plate spline). The implementation of the method, the results and the conclusions are also presented.

6.2 LITERATURE REVIEW

Thin plate splines are widely used as an interpolation function and have been commonly used as a tool in computer vision applications. The goal of this work is to implement a three-dimensional interpolation thin plate spline algorithm and a smoothing thin plate spline algorithm

for image warping of magnetic resonance imaging. Very little literature has been developed for the thin plate spline method, specifically in three dimensions, for medical image warping. Bookstein (1989) first proposed the use of a two-dimensional thin plate spline for point-based registration for medical imaging. Rohr et al. (1996) developed an approximation thin plate spline method based on regularization theory to account for landmark localization errors. Johnson et al. (2002) developed two approaches for image registration based on thin plate splines. The first approach provides a method that can be used to estimate a consistent pair of forward and reverse transformation given a set of corresponding landmarks. The second approach combines landmark and intensity information to estimate a consistent pair of forward and reverse transformations. Evans et al. (1991) described a tool for segmenting brain image volumes through analytic transformations of a 3D computerized volume-of-interest atlas to fit individual datasets. The contribution of this work will include borrowing Bookstein and Rohr's thin plate spline methods and extending them to develop a three-dimensional interpolation thin plate spline method. In addition, we performed smoothing thin plate spline method in two-dimensions.

6.3 THIN PLATE SPLINES REVIEW

A spline is a function defined by piecewise polynomials with pieces smoothly connected together. The joining points of the polynomial pieces are called knots and they do not have to be evenly spaced. Splines are very useful for modeling arbitrary functions, and are widely used in statistics and computer graphics. There are several types of splines for data interpolation and smoothing of one-dimensional or multi-dimensional data. Spline interpolation is a type of

interpolation where the interpolant is a spline. Smoothing splines are a method of fitting a smooth curve to a set of noisy observations.

6.3.1 Thin Plate Spline Review

6.3.1.1 Interpolation Thin Plate Spline

A thin plate spline (TPS) is a smooth function that interpolates a surface that is fixed at the landmark points p_i. In morphometrics, a landmark point is a discrete point that defines the same area among all of the forms of a data set (Bookstein, 1991). The landmark points can be defined either manually or automatically.

The following notation is derived from Bookstein (1989). The TPS algorithm fits a mapping function $f(x)$ between corresponding landmark points by minimizing the bending energy function $J_m^d(f)$ involving m derivatives in d-dimensions. The penalty functional for two dimensions $J_2^2(f),\ d=2, m=2$ is defined as

$$J_2^2(f) = \int_{-\infty}^{\infty}\int_{-\infty}^{\infty}\left(\frac{\partial^2 f}{\partial x^2}\right)^2 + 2\left(\frac{\partial^2 f}{\partial x \partial y}\right)^2 + \left(\frac{\partial^2 f}{\partial y^2}\right)^2 dxdy. \tag{6.1}$$

For three dimensions, the thin plate spline penalty functional $J_2^3(f)$ is defined as

$$J_2^3(f) = \int_{-\infty}^{\infty}\int_{-\infty}^{\infty}\left(\frac{\partial^2 f}{\partial x^2}\right)^2 + \left(\frac{\partial^2 f}{\partial y^2}\right)^2 + \left(\frac{\partial^2 f}{\partial z^2}\right)^2 + 2\left[\left(\frac{\partial^2 f}{\partial x \partial y}\right)^2 + \left(\frac{\partial^2 f}{\partial x \partial z}\right)^2 + \left(\frac{\partial^2 f}{\partial y \partial z}\right)^2\right] dxdydz. \tag{6.2}$$

The penalty functional measures the overall roughness of the function f. The bending energy is invariant under affine transformations like scaling, rotation and translation. This property makes it suitable to provide a quantitative measure of deformations. A thin plate spline function for two-dimensions is defined as

$$f(x,y) = a_1 + a_x x + a_y y + \sum_{i=1}^{n} w_i U\left(\left| p_i - (x,y)\right|\right), \tag{6.3}$$

where $U(r) = r^2 \log r^2$ is the fundamental solution of the biharmonic equation (basis functions), $r = \left(x_i - x_j\right)^2 + \left(y_i - y_j\right)^2$, $|\cdot|$ indicates length of a vector, the p_i are the landmark points that the TPS interpolates, a_1, a_x, a_y define the affine part of the transformation and w_i define the nonlinear deformation. This model is able to represent elastic deformations (Bookstein, 1989).

A special function in spline analysis is $z(x,y) = U(r) = r^2 \log r^2$, where r is the distance $\sqrt{x^2 + y^2}$ from the Cartesian origin. The function $U(r)$ satisfies the following equation

$$\Delta^2 U = \left(\frac{\partial^2}{\partial x^2} + \frac{\partial^2}{\partial y^2} \right)^2 U \propto \delta_{(0,0)}, \tag{6.4}$$

where the function U is the fundamental solution of the biharmonic equation $\Delta^2 U = 0$, the equation for the shape of a thin plate lofted as a function $z(x,y)$ above the (x,y) plane. The TPS can be easily extended to three-dimensional data. For three dimensions, the fundamental solution of the biharmonic equation is

$$U(r) = |r|. \tag{6.5}$$

The general problem for three dimensions can be stated as follows: let $p_1 = (x_1, y_1, z_1), p_2 = (x_2, y_2, z_2), \ldots, p_n = (x_n, y_n, z_n)$ be n landmark points in the Euclidean space, according to a convenient Cartesian coordinate system. Define the following matrices

$$K = \begin{bmatrix} 0 & U(r_{12}) & \cdots & U(r_{1n}) \\ U(r_{21}) & 0 & \cdots & U(r_{2n}) \\ \cdots & \cdots & \cdots & \cdots \\ U(r_{n1}) & U(r_{n2}) & \cdots & 0 \end{bmatrix}_{n \times n}, \tag{6.6}$$

$$P = \begin{bmatrix} 1 & x_1 & y_1 & z_1 \\ 1 & x_2 & y_2 & z_2 \\ \dots & \dots & \dots & \dots \\ 1 & x_n & y_n & z_n \end{bmatrix}_{n\times 4}, \tag{6.7}$$

and

$$L = \begin{bmatrix} K & P \\ P^T & O \end{bmatrix}_{(n+4)\times(n+4)}, \tag{6.8}$$

where $r_{ij} = \left| p_i - p_j \right|$ defines the distance between points i and j, $U(r_{ij})$ as defined above, n is the number of landmark points, ^{T} denotes the matrix transpose and O is a 4×4 matrix of zeros. Also, let V be a $3\times n$ matrix defined as

$$V = \begin{bmatrix} x_1' & x_2' & \dots & x_n' \\ y_1' & y_2' & \dots & y_n' \\ z_1' & z_2' & \dots & z_n' \end{bmatrix}, \tag{6.9}$$

where each (x_i', y_i', z_i') is a point homologous to (x_i, y_i, z_i) in another copy of $\Re^3$. Then, define $V = (v_1, \dots, v_n)$ as an $n-$vector and Y as column vector of length $n+4$, $Y = (V \mid 0000)^T$. The vector of weights $W = (w_1, w_2, \dots, w_n)$ and the coefficients a_1, a_x, a_y, a_z are defined by the following equation

$$L^{-1}Y = (W \mid a_1 a_x a_y a_z)^T. \tag{6.10}$$

The elements of $L^{-1}Y$ are used to define a function $f(x, y, z)$ everywhere in the plane

$$f(x, y, z) = a_1 + a_x x + a_y y + a_z z + \sum_{i=1}^{n} w_i U\left(\left| p_i - (x, y, z) \right|\right). \tag{6.11}$$

This function maps each point (x_i, y_i, z_i) to its homologous (x_i', y_i', z_i') and is least bent. The first four terms describe the affine transformation and the other term describes the nonlinear transformation.

6.3.1.2 Smoothing Thin Plate Splines

When applying an interpolating TPS method, a transformation is determined, which maps the source and the target landmarks points exactly. This method assumes that the positions of the landmark points are known exactly. However, the position of the landmarks points can only be approximated. Therefore, an interpolating thin plate spline is not adequate. To take into account the landmark localization errors one has to weaken the interpolation condition. This can be done by combining the bending energy in Equation 6.1 (or Equation 6.2 for three dimensions) and an approximation scheme. This approximation method is based on the mathematical work of Wahba (1990). A two dimensional smoothing thin plate spline is the solution to the following problem

$$J_\lambda(f) = \frac{1}{n}\sum_{i=1}^{n}(p_i - f(x,y))^2 + \lambda J(f), \tag{6.13}$$

where $\lambda > 0$ is the smoothing parameter. The minimization of this function yields a transformation f that approximates the distance between the landmark points and is sufficiently smooth. The trade-off between fidelity of the data and smoothness of the transformation is determined by the smoothing parameter. When $\lambda = 0$, we obtain a full interpolation method, while for large λ, there is only an affine transformation. The addition of this term results in a better conditioned system of linear equations than in the case of the interpolation thin plate spline approach. One way to calibrate the amount of smoothing is by determining the effective degrees of freedom defined by $df = tr(S)$ (Hastie and Tibshirani, 1990). Craven and Wahba (1979) also

developed a method, generalized cross-validation (GCV), for estimating the optimum amount of smoothing from the data using smoothing splines. GCV is a weighted least squares cross validation defined by

$$GCV(\alpha) = \frac{1}{n}\sum_{i=1}^{n}\left\{y_i - \hat{f}_{\alpha}^{-i}(x_i)\right\}^2 w_i(\alpha), \tag{6.14}$$

where $w_i(\alpha)$ are the weights chosen to reflect unequally spaced data and are defined as

$$w_i(\alpha) = \left[\frac{(1 - S_{ii}(\alpha))}{\frac{1}{n}tr(I - S(\alpha))}\right]^2, \tag{6.15}$$

where $i = 1,\ldots,n$, $S_{ii}(\alpha)$ are the diagonal elements of the smoothing matrix $S(\alpha)$ and I is the identity matrix. The GCV estimate can be written in matrix notation as

$$GCV(\alpha) = \frac{\frac{1}{n}\left\|(I - S(\alpha))y\right\|^2}{\left(\frac{1}{n}tr(I - S(\alpha))\right)^2}, \tag{6.16}$$

where $\|I - S(\alpha)y\|$ defines the norm of $I - S(\alpha)y$.

6.4 IMPLEMENTATION

Interpolating thin plate splines were computed in MATLAB Software (The MathWorks, Inc., 1994-2008). To load and save ANALYZE format images we used the NIFTI/ANALYZE image tool in MATLAB. The three-dimensional interpolating TPS procedure was used to fit MRI brain images from one healthy control to the standard MNI template in SPM. The template was a young structural template that was created from images of 152 healthy subjects (23.4 ± 4.1

years) at the Montreal Neurological Institute (MNI) that is the current standard template in SPM. The original MR images have dimensions 160 x 180 x 170 voxels. The template has dimension 91 x 109 x 91 voxels. Interpolation TPS was applied to the MR image in order to obtain the MR on the same space as the template and to match each data volume from the subject's MR to the template. After applying interpolation TPS, the anatomic structures in the subject's image should match the anatomic structures in the template.

For the smoothing thin plate spline, affine transformation was performed in SPM2 (Wellcome Department of Imaging Neuroscience, London, UK, 2007). Smoothing thin plate splines was performed in R Software (The R Project for Statistical Computing, http://www.r-project.org/). To fit the thin plate spline in R we used the *rgcvpack* package. This package allows the fitting of smoothing thin plate splines of any order with user specified knots. In addition, the *fields* package was used to evaluate each fit. The AnalyzeFMRI package in R was used to read (image volumes and image slices) and write ANALYZE format images.

For the smoothing TPS, we fit an adaptive smoothing thin plate spline to overlapping blocks of a MR image slice, and blended the splines together smoothly. Xie et al. (2006) used a similar idea for image segmentation. Details of the implementation are given as follows. First, an affine transformation was applied to the structural Magnetic Resonance (MR) image data (size 160x180x170 pixels) to account for differences in position, orientation and overall brain size. After affine transformation, each image slice (size 91x109 pixels) was divided into overlapping blocks of size 40x40 pixels. The overlapping proportion between each pair of horizontally and vertically adjacent blocks is about 35-50 percent and 35-38 percent of the pixels, respectively. The overlapping scheme of each slice was three (horizontally) by four

(vertically) blocks. The template image was also divided into overlapping blocks of size 40x40 pixels.

After defining the blocks, we fit a smoothing thin plate spline to each block with all data points as knots. In addition, we fit a smoothing thin plate spline to each block using a subset of the knots (1600 knots). The smoothing parameter λ for each fit was chosen by generalized cross validation. The optimal number of knots for each block was determined by minimizing the sum of squared intensity differences between the subject's image intensities and template intensities. Given the optimal number of knots, we fit a thin plate spline to each block. Then, the thin plate spline was predicted on the regular grid. After fitting and predicting the thin plate spline for each block, we blended the blocks (images) together using the sum of squared differences as weights. When the blocks are blended together, the image was ready to be saved as normalized images.

6.4.1 Human Subjects

Fourteen healthy control (Control), sixteen type 2 diabetic (Diabetes) and eight depressed type 2 diabetic (Depressed Diabetes) subjects were recruited for a positron emission tomography imaging study as described (Price et al., 2002, 2003; Rosario et al. 2008). The present work focuses only on the structural MR image data that were acquired to guide region-of-interest determination and partial volume correction. This work will be applied to the structural MR image data from a healthy control subject.

6.4.2 Magnetic Resonance Imaging

6.4.2.1 Image Acquisition

Magnetic resonance imaging was performed on a 1.5 Tesla G.E. Signa system. All subjects were positioned in a standard head coil and a brief scout T1-weighted image was obtained. The axial series was acquired (oriented to the anterior and posterior commissures) to screen subjects for unexpected pathology: fast spin-echo T2-weighted (effective TE=102, TR=2500, NEX=1, slice thickness=5mm/1mm interslice) and proton density weighted images (effective TE=17, TR=2000, NEX=1, slice thickness=5 mm/1mm interslice). A field of view of 24 cm and image matrix of 256x192 pixels were used for all axial MR series. A volumetric spoiled gradient recall (SPGR) sequence with parameters optimized for maximal contrast among gray matter, white matter, and CSF was acquired in the coronal plane (TE=5, TR=25, flip angle=40 degrees, NEX=1, slice thickness=1.5 mm/0mm interslice). All MR image data analyzed were skull stripped manually using ANALYZE AV. All MR images were AC-PC (anterior commissure-posterior commissure) aligned before applying the proposed method.

6.4.2.2 Landmark Location

For illustrating the interpolation TPS method, thirteen specific anatomical landmark points were identified in each subject's MR space and template. The anatomical landmarks included: anterior and posterior commissure, genu of corpus callosum, most superior point of the central sulcus, most inferior point of the caudate, most superior/posterior and most inferior/anterior points of the parieto-occipital sulcus, most frontal/posterior cingulate sulcus, meeting point of the fourth ventricle, most posterior point of the Sylvian fissure and most inferior point (left/right) of the temporal occipital lobe. To localize the specific landmark coordinates we used SPM5.

6.4.3 Results

Interpolation and smoothing thin plate splines were applied to perform spatial normalization (image warping) of a healthy control subject magnetic resonance (MR) image to a standard template. Figure 33 shows the subject's MRI, which has dimensions 160 x 180 x 170 and Figure 34 A and B shows the standard template and atlas used to perform the image warping. We apply an interpolation thin plate spline on the coordinates of 13 landmarks, defined in Section 6.4.2.2, to map each coordinate in the template to its homologous in the subject's image and to obtain linear and nonlinear parameters. Then, the interpolation TPS function was applied to each image's coordinates to obtain the new coordinates in the standard space. Interpolation TPS results show that this method is not appropriate to perform spatial normalization of three-dimensional MR image to a standard template since the image appears to be stretched (Figure 34-C, coronal (top), sagittal (middle) and axial view(bottom)). That is, the warped image has the same dimensions as the template, due to affine transformation, but the anatomical regions in the template do not match the anatomical regions in the warped image. Smoothing TPS results show that an adaptive smoothing TPS method might not be applicable for spatial normalization since it tends to smooth the images at a greater extent (Figure 34-D).

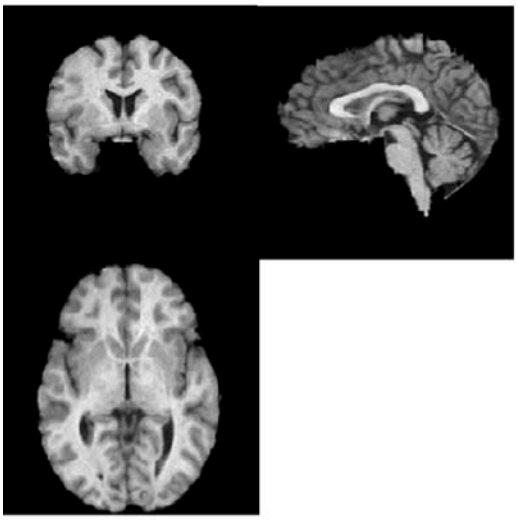

Figure 33 Magnetic Resonance Image for a healthy control subject (coronal, sagittal and axial views). Image dimensions: 160 x 180 x 170.

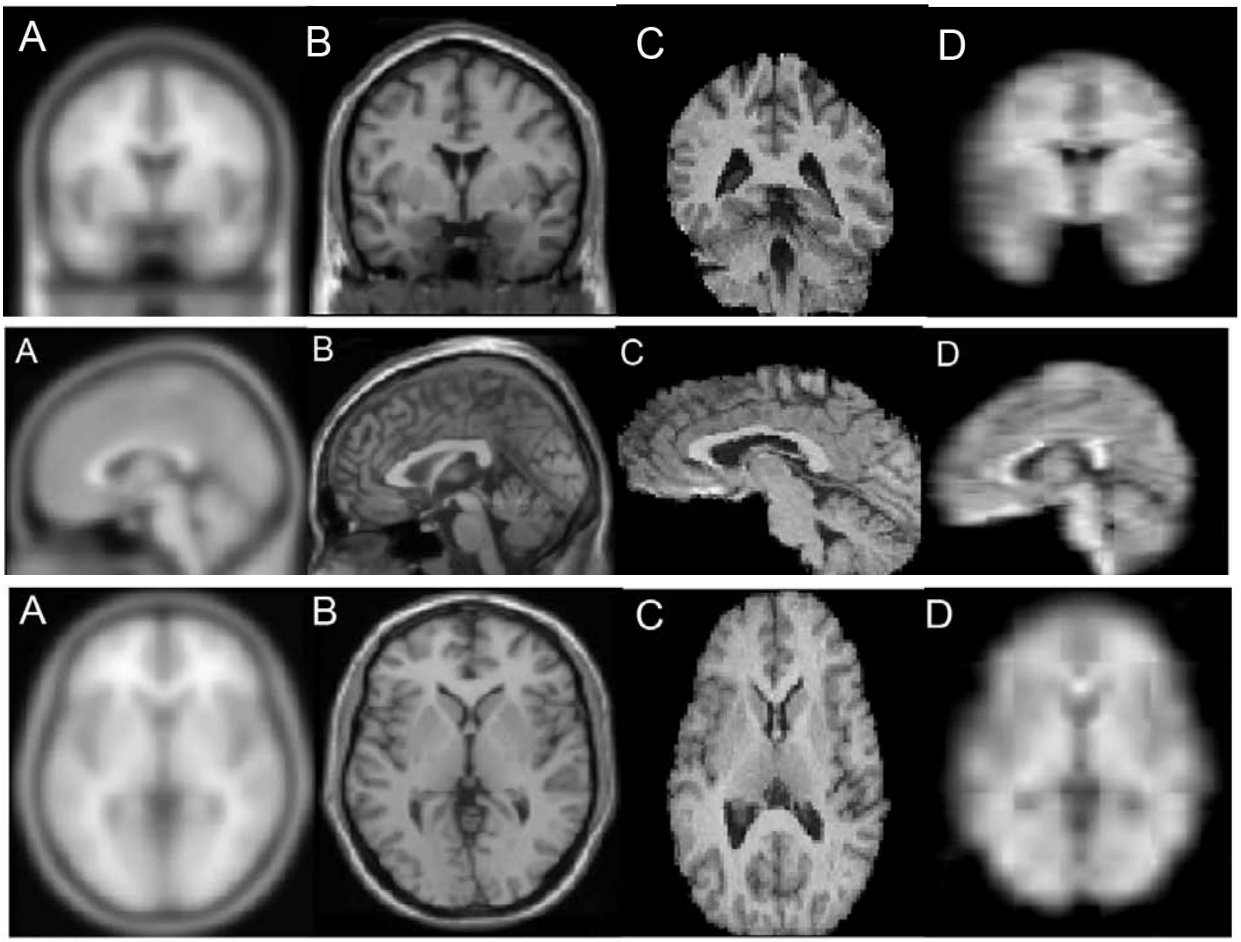

Figure 34 Coronal (top), sagittal (middle) and axial views (bottom). (A) Standard template in SPM, (B) Atlas from the standard template in SPM, (C) Results for the interpolation TPS. (D) Results from the Smoothing TPS. All images have dimensions 91 x 109 x 91.

6.5 CONCLUSIONS AND DISCUSSION

Spatial normalization is an essential imaging pre-processing step for voxel-based analyses of brain imaging data, since this step ensures that data from different subjects are derived from homologous regions in the brain. The current work proposes a three-dimensional interpolation thin plate spline method and a two-dimensional smoothing thin plate spline method for image warping of magnetic resonance imaging. These methods have the advantage that the parameters do not require manual tuning. A drawback from the interpolation thin plate spline method is that definition of landmarks has to be performed by an experienced person. Results for the interpolation thin plate spline method show that this method might not be optimal for spatial normalization of images in three-dimensions. This outcome can be a result of the definition of the landmark points and/or the small amount of landmarks points used in the method. Results from the smoothing thin plate spline method show that this method might not be optimal for image warping since the resulted image tends to be very smooth. Therefore, the interpolation and smoothing thin plate splines methods are not suitable to performed image warping of magnetic resonance imaging to a standard template. Future work will include quantitative analyses and modification of the thin plate spline methods.

APPENDIX A

Paper -- Assessment of parameter settings for SPM5 spatial normalization of structural MRI data: Application to type 2 diabetes

Rosario, B.L., Ziolko, S.K., Weissfeld, L.A., Price, J.C., 2008. *NeuroImage* 41: 363-370.

ELSEVIER

NeuroImage

www.elsevier.com/locate/ynimg
NeuroImage 41 (2008) 363–370

Technical Note

Assessment of parameter settings for SPM5 spatial normalization of structural MRI data: Application to type 2 diabetes

Bedda L. Rosario,[b,*] Scott K. Ziolko,[a] Lisa A. Weissfeld,[b] and Julie C. Price[c]

[a]*Department of Radiology, University of Pittsburgh School of Medicine, Presbyterian University Hospital, 200 Lothrop Street, Pittsburgh, PA 15213, USA*
[b]*Department of Biostatistics, University of Pittsburgh, Graduate School of Public Health, 130 DeSoto Street, 326 Parran Hall, Pittsburgh, PA 15261, USA*
[c]*Department of Radiology, University of Pittsburgh School of Medicine, Presbyterian University Hospital, B-938, 200 Lothrop Street, Pittsburgh, PA 15213,USA*

Received 3 August 2007; revised 4 February 2008; accepted 8 February 2008
Available online 15 February 2008

Spatial normalization is the process of standardizing images of different subjects into the same anatomical space. The goal of this work was to assess standard and unified methods in SPM5 for the normalization of structural magnetic resonance imaging (MRI) data acquired in mid-life/elderly subjects with diabetes. In this work, we examined the impact of different parameters (i.e. nonlinear frequency cutoff, nonlinear regularization and nonlinear iterations) on the normalization, in terms of the residual variability. Total entropy was used to assess the residual anatomical variability after spatial normalization in a sample of 14 healthy mid-life/elderly control subjects and 24 mid-life/elderly subjects with type 2 diabetes. Spatial normalization was performed using default settings and by varying a single parameter or a combination of parameters. Descriptive statistics and nonparametric tests were used to examine differences in total entropy. Statistical parametric mapping analyses were performed to evaluate the influence of parameter settings on the spatial normalization. Total entropy results and SPM analyses suggest that the best parameters for the spatial normalization of mid-life/elderly image data to the MNI template, when applying the standard approach, correspond to the default cutoff (25 mm), heavy regularization, and the default number of nonlinear iterations (16). On the other hand, when applying the unified approach, the default parameters were the best for spatial normalization of mid-life/elderly image data to the MNI priors. These findings are relevant for studies of structural brain alterations that may occur in normal aging, chronic medical conditions, neuropsychiatric disorders, and neurodegenerative disorders.

Keywords: Statistical parametric mapping; Spatial normalization; Residual variability; Total entropy; Type 2 diabetes

Introduction

Magnetic resonance (MR) imaging is a technique that is widely used to generate images of brain structure and/or function. One way of analyzing imaging data consists of comparing brain images between subjects on a voxel-wise basis. These comparisons require that all brain structures occupy the same standard anatomical space in a consistent manner. To achieve this, an image-processing step known as spatial normalization is applied. This step is required to ensure that homologous regions in the brain are comparable across subjects before performing subsequent analyses.

Several techniques are available to perform spatial normalization. The most widely used normalization software in the research literature is Statistical Parametric Mapping (SPM). Most researchers choose to use the default parameter settings for spatial normalization in SPM when conducting their studies. An advantage of using the default parameters is that brain images can be compared across different studies. On the other hand, a disadvantage is that the default parameter set might not be the best choice for spatial normalization of images-of-interest to a standard space.

Several studies (e.g. Meyer et al., 1999; Sugiura et al., 1999; Crivello et al., 2002; Gispert et al., 2003; Hellier et al., 2003; Robbins et al., 2004; Hosaka et al., 2005; Wu et al., 2006, Crinion et al., 2007) have compared and assessed different spatial normalization procedures. In addition, the precision of the spatial normalization in SPM has been assessed in terms of anatomical landmarks (Crinion et al., 2007; Salmond et al., 2002). Nearly all previous studies have focused on healthy and young subjects as opposed to diseased and elderly subjects, with the exception of Salmond et al. (2002) and Gispert et al. (2003), who respectively focused on bilateral hippocampal atrophy patients and schizophrenic patients. Crinion et al. (2007) also examined simulated brain lesions.

Spatial normalization involves applying a spatial transformation that moves and warps images into the same standard anatomical space defined by a template. The objective of normalization is to remove, to some extent, anatomical variability between the subjects' images to allow subsequent analysis of the data. Spatial normal-

* Corresponding author. Fax: +1 412 624 2183.
E-mail addresses: blr5@pitt.edu (B.L. Rosario), lweis@pitt.edu (L.A. Weissfeld), pricejc@upmc.edu (J.C. Price).
Available online on ScienceDirect (www.sciencedirect.com).

1053-8119/$ - see front matter © 2008 Elsevier Inc. All rights reserved.
doi:10.1016/j.neuroimage.2008.02.004

ization is a critical step in the analysis of brain imaging data since it produces the "raw" data for the subsequent analyses. Therefore, it is important to study and understand how spatial normalization in SPM works under different conditions and parameter settings.

The purpose of this comparative study was to assess how changes in parameter settings in SPM affect the performance of spatial normalization, by examining the residual variability of normalized image data across three groups of mid-life/elderly subjects who were healthy controls, non-depressed diabetics and depressed diabetics. Structural brain alterations, such as brain atrophy and changes in ventricle size, were expected to occur to a greater extent for these subjects than for younger subjects. In particular, we were interested in how the nonlinear frequency cutoff, the nonlinear regularization and the number of nonlinear iterations, affect the residual variability of normalized structural MR imaging data. Because of the difficulty of defining a gold standard for parameter settings in SPM, we define the default parameters as the gold standard. In addition, we will compare total entropy results using two approaches: SPM5 standard method and SPM5 unified method.

Materials and methods

Human subjects

Fourteen healthy control (Control), sixteen type 2 diabetic (Diabetes) and eight depressed type 2 diabetic (Depressed Diabetes) subjects were recruited for a positron emission tomography imaging study (Price et al., 2002, 2003). The present work focuses only on the structural MR data that were acquired to guide region-of-interest determination and partial volume correction. Only a brief description of the participant recruitment and characteristics will therefore be provided. Table 1 describes the subject characteristics including age and gender. Subjects were recruited through university collaborations that included the University of Pittsburgh Obesity and Nutrition Research Center and Intervention Research Center for Late-life Mood Disorders, as approved by the Biomedical Institutional Review Board. None had a history of substance abuse or dependence. Exclusion criteria included medical or neurological illnesses likely to affect brain physiology or anatomy, suicidal intent, and exposure to psychotropic or other medications. Subjects were excluded if they were currently on antidepressants, taking insulin, or had major medical complications (peripheral vascular disease-CAD, PVD, CVA/TIA; history of stroke), or complex medical regimens. The glycosylated hemoglobin index of diabetes was measured for 10/14 controls (5.6±0.3%) and all diabetics (non-depressed: 7.1±1.2%; depressed: 7.5±1.5%). The Hamilton Depression Inventory averaged 1.6±1.6 for controls to 18.6±4.4 for the depressed diabetics.

Table 1
Subject Demographics

Group	Age (years)	Gender (M:F)
Control		
$n=14$	62.14±13.00	6:8
Diabetes		
$n=16$	55.94±9.33	9:7
Depressed diabetes		
$n=8$	62.75±10.61	3:5

Magnetic resonance imaging

Magnetic resonance imaging was performed on a 1.5 Tesla G.E. Signa system. All subjects were positioned in a standard head coil and a brief scout T1-weighted image was obtained. The axial series was acquired (oriented to the anterior and posterior commissures) to screen subjects for unexpected pathology: fast spin-echo T2-weighted (effective TE=102, TR=2500, NEX=1, slice thickness=5 mm/1 mm interslice) and proton density weighted images (effective TE=17, TR=2000, NEX=1, slice thickness=5 mm/1 mm interslice). A field of view of 24 cm and image matrix of 256x192 pixels were used for all axial MR series. A volumetric spoiled gradient recall (SPGR) sequence with parameters optimized for maximal contrast among gray matter, white matter, and CSF was acquired in the coronal plane (TE=5, TR=25, flip angle=40°, NEX=1, slice thickness=1.5 mm/0 mm interslice). All MR image data analyzed were skull stripped manually using ANALYZE AV.

Spatial normalization

SPM5 Standard Method

The standard normalization method in SPM5 minimizes the sum of squared differences between the subject's image and the template, while maximizing the prior probability of the transformation. This spatial normalization begins by determining the optimum twelve-parameter affine transformation to account for differences in position, orientation and overall brain size. After affine transformation, a nonlinear transformation is applied to correct for gross differences in head shape that were not accounted for by the affine transformation. The nonlinear deformations are described by the lowest frequency components of a three-dimensional discrete cosine transform basis functions (Ashburner and Friston, 1999).

For the standard method, the user has the ability to select parameter estimation settings for the nonlinear transformation. We will focus on three parameter estimation settings: nonlinear frequency cutoff, nonlinear regularization and the number of nonlinear iterations.

Nonlinear Frequency Cutoff represents the cutoff (mm) of the period of the cosine basis functions. SPM will only estimate warps of the order of the specific "cutoff" or larger. Smaller cutoff values represent the use of a larger number of basis functions that result in greater warping along each axis. The default for nonlinear transformation in SPM is 25 mm.

Nonlinear Regularization is the inclusion of a log-likelihood penalty term for unlikely deformations. Greater regularization provides smoother deformations. The smoothness measure is determined by the bending energy of the deformations. The default value for degree of regularization in SPM is medium regularization (1).

Nonlinear Iterations is the number of iterations performed during the parameter estimation process. The default number for nonlinear iterations in SPM is 16.

SPM5 Unified Method

The new SPM5 method combines segmentation, spatial normalization and bias correction in a unified model approach (Ashburner and Friston, 2005). Spatial normalization begins with an affine transformation to achieve an approximate alignment. Then, deformation of the tissue probability maps is performed to achieve a better model fit to the data. Similar to the standard method, the unified model option allows the user to choose different values of the warp frequency cutoff and warping regularization.

Segmentation

The SPM segmentation of structural MR brain images generates probability maps for the following tissue types: gray matter (GM), white matter (WM) and cerebrospinal fluid (CSF). The segmentation method in SPM5 is based upon a Gaussian mixture model, provides an intensity non-uniformity (or bias) correction and implements deformable tissue probability maps (Ashburner and Friston, 2005).

Total entropy

Total entropy is a measure that can be used to assess the amount of uncertainty associated with a random variable and has been used by others to assess the residual variability remaining after spatial normalization (Warfield et al., 2001; Robbins et al., 2004).

Assume V is a discrete random variable that represents the distribution of tissue types for a given voxel v. Let $p(v)=\Pr\{V=v\}$, $t\in T$, where v denotes the voxel, T is the set of possible tissue types that define the probability distribution at voxel v, and $p_t(v)$ is the probability that voxel v is of tissue type t (i.e., GM, WM or CSF) based upon the segmentation of the normalized MR images. The entropy of a random variable V (Cover and Thomas, 2006) is defined by

$$H_b(v) = -\sum_{v\in V} p_t(v)\ \log_b\ p_t(v), \tag{1}$$

where $0\cdot\log_2\cdot 0$ is defined to be zero. The total entropy is thus defined over all voxels as:

$$H_b = \sum_{v} H_b(v). \tag{2}$$

For the purpose of this work, the entropy of V is measured in base b units that will correspond to logarithm base 2 (i.e. H_2), and the measurement of entropy in bits. Entropy was calculated for each subject's normalized segmented image in a voxel-wise manner, based upon Eq. (1):

$$H_2(v) = -\sum_{t\in T} p_t(v)\ \log_2\ p_t(v). \tag{3}$$

According to Eq. (1), a large amount of uncertainty can reflect more information and hence a greater entropy. Total entropy is zero when a spatial normalization achieves complete matching of homologous regions of a subject's brain to the template; or when there is a distribution where each label is equally likely. Ideally, one would like to find a combination of parameter settings in SPM that minimizes the total entropy. That is, smaller total entropy is assumed to generally reflect less uncertainty and therefore better spatial normalization.

Study design

Spatial normalization (standard and unified methods) was performed using SPM5 software (Wellcome Department of Imaging Neuroscience, London, UK, 1994–2007). All normalized images were written out using the template-bounding box and voxel size of 2 mm. Prior to calculation of total entropy, each normalized segmented MR image was smoothed using an 8-mm FWHM Gaussian isotropic kernel.

SPM5 standard method

Firstly, each subject's MR data was spatially normalized to the standard MNI (Montreal Neurological Institute) template in SPM using the standard approach, varying a single parameter at a time while setting all other parameters to the default. The normalization parameter settings were nonlinear frequency cutoff (affine only, 25 mm, 45 mm and 70 mm), nonlinear regularization (light, medium and heavy) and nonlinear iterations (3, 8 and 16). Secondly, the standard method (with the MNI template) was applied to each subject's MR by varying a combination of parameters for nonlinear frequency cutoff and nonlinear regularization to determine how the relationship of these two parameters affects the performance of the normalization. After each spatial normalization, segmentation was applied to the normalized images and total entropy (see Eqs. (1)–(3)) was calculated using the GM, WM and CSF image data.

SPM5 unified method

The unified segmentation was also applied to each subject's MR data (default tissue priors in SPM), varying a single parameter at a time while setting all other parameters to the default. The parameter settings were: warp frequency cutoff (affine only, 25 mm, 45 mm and 70 mm) and warping regularization (light, medium and heavy). In contrast to the standard method, the unified segmentation produces modulated normalized segmented images of GM, WM and CSF. In addition, the unified method was applied to each subject's MR using a combination of parameters for warp frequency cutoff and warping regularization to determine how the relationship of these two parameters affects the performance of the spatial normalization.

Statistical analysis

Total entropy data were analyzed for each subject group in SPSS 14 (SPSS Inc.) to provide descriptive statistics (including box plots) and to perform nonparametric testing for two-related or three-related samples (e.g. comparison across three different frequency cutoffs). Each box plot indicates minimum value, lower quartile (lowest 25% of data), median, upper quartile (highest 25% of data) and maximum value. Open circles indicate outliers that were either 1.5 fold less than the first quartile or 1.5 fold greater than the third quartile. Stars indicate outliers that were either 3 fold less than the first quartile or 3 fold greater than the third quartile. The nonparametric tests were used to examine differences in total entropy that might arise from different levels of frequency cutoff, regularization or number of nonlinear iterations. If the three-related samples test indicated statistically significant differences, a paired t-test was performed to compare the "minimum" and "default" total entropy results for that parameter set. To assess the extent to which differences in the normalization results could influence subsequent analyses of the MR data, paired t-tests were performed in SPM. The paired t-tests compared normalized MR data obtained by using the default parameter settings to the normalized MR data for which the total entropy was lowest (contrast [−1 1]). The SPM analyses were only performed for the control MR data. The SPM significance threshold was set to a FDR corrected p-value of $p<0.001$ and an extent threshold of 50 voxels.

Results

Total entropy

SPM5 standard method (SM)

Spatial normalization performed using affine transformation resulted in smaller total entropy, relative to all nonlinear transformation results (Fig. 1A, bottom). The difference between the mean total entropy values determined using an affine transformation and a nonlinear transformation with default parameters was approximately

6% for all three subject groups. The mean total entropy for affine transformation for controls, diabetics and depressed diabetics using the standard method was 1.93×10^5 (s.d.=0.10), 1.98×10^5 (s.d.=0.10) and 2.05×10^5(s.d.=0.05) bits respectively.

Nonlinear frequency cutoff (SM). A frequency cutoff of 70 mm tended to give lower total entropy, when compared to smaller cutoff values. This finding held true for all groups. Total entropy results for different levels of the frequency cutoff are shown in Fig. 1A (bottom). The mean entropy for the smallest frequency cutoff of 25 mm (default) for controls, diabetics and depressed diabetics was 2.06×10^5 (s.d.=0.11), 2.13×10^5 (s.d.=0.10) and 2.18×10^5 (s.d.=0.07) bits, respectively, while that for the largest cutoff setting (70 mm) was 2.01×10^5 (s.d.=0.10), 2.07×10^5 (s.d.=0.11) and 2.14×10^5 (s.d.=0.06) bits, respectively. The difference in the mean total entropy value between 25 mm and 70 mm was only about 2–3%.

Nonlinear regularization (SM). The total entropy results show that increases in the regularization for the nonlinear transformation (when using the standard method in SPM5) reduces the residual variability (Fig. 1B, bottom). Heavy regularization yielded lower residual variability when compared to medium regularization (default). This finding held true for all groups. The mean entropy for heavy regularization for controls, diabetics and depressed diabetics was 2.00×10^5 (s.d.=0.11), 2.06×10^5 (s.d.=0.09) and 2.11×10^5 (s.d.=0.06) bits respectively, while the mean entropy for medium regularization for controls, diabetics and depressed diabetics was 2.06×10^5(s.d.=0.11), 2.13×10^5(s.d.=0.10) and 2.18×10^5 (s.d.=0.07) bits respectively. The difference in mean entropy value between smallest and largest regularization was approximately 3% for all groups.

Combination of nonlinear frequency cutoff and nonlinear regularization (SM). Fig. 2 (top) shows that when combining different levels of nonlinear cutoff and nonlinear regularization the total entropy changes. As the frequency cutoff increases, the effect of nonlinear regularization on the spatial normalization decreases. That is, regularization of a larger nonlinear frequency cutoff had little mean effect. This was seen for all three cutoffs evaluated (including 45 mm), although results for two are shown in Fig. 2 for clarity.

Nonlinear iterations (SM). Total entropy results show that smaller number of nonlinear iterations led to smaller residual variability for the standard approach in SPM5. A nonlinear iteration number of three tended to provide smaller residual variability relative to the default (16 iterations). These results are shown in Fig. 3. The mean entropy for three iterations for controls, diabetics and depressed diabetics was 2.04×10^5(s.d.=0.10), 2.10×10^5 (s.d.=0.10) and 2.15×10^5 (s.d.=0.07) bits respectively and 2.06×10^5(s.d.=0.11), 2.13×10^5(s.d.=0.10) and 2.18×10^5 (s.d.=0.07) bits respectively, for the default setting. However, the difference in the mean total entropy value was only about 1% for all three groups.

Nonparametric statistical results. Our results indicate that there are differences in residual variability when parameter settings change in the nonlinear transformation using the standard approach for this

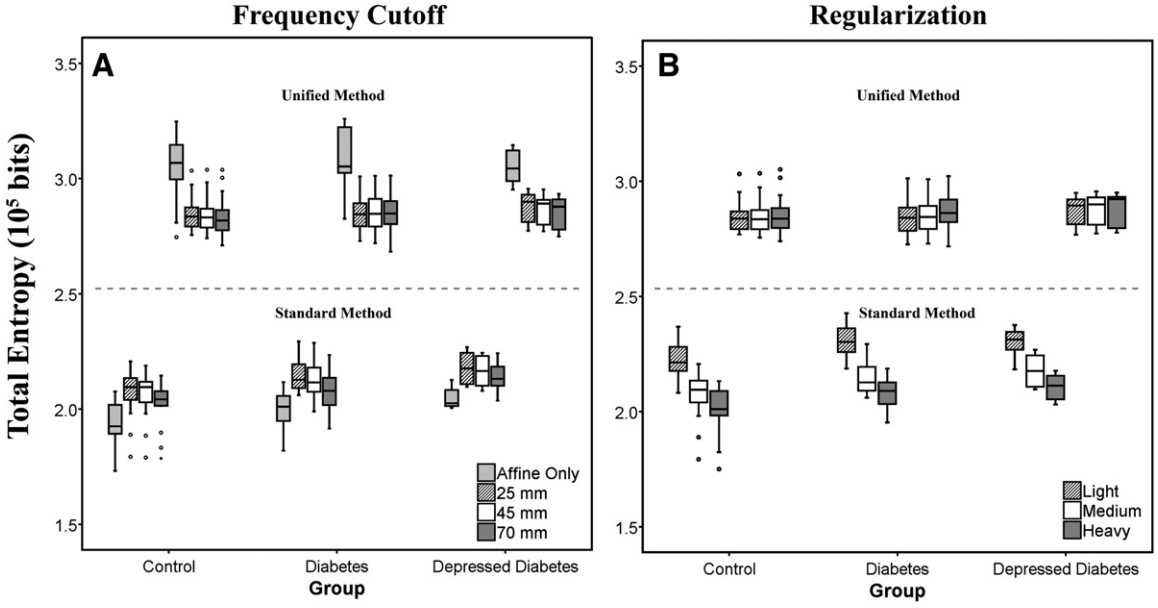

Fig. 1. Residual variability (i.e., total entropy) for normalizations performed by varying a single parameter at a time, while all other parameters were fixed to their default value, for both SPM5 methods (top: unified, bottom: standard). (A) Affine transformation and nonlinear transformations that correspond to nonlinear frequency cutoff of 25 mm*, 45 mm or 70 mm. (B) Normalizations were performed using light, medium* or heavy regularization. For the standard method, an affine transformation resulted in the lowest total entropy relative to the nonlinear. In addition, a larger frequency cutoff or heavy regularization provided significantly lower residual variability for nonlinear normalization when applying the standard approach. For the unified method, a nonlinear transformation resulted in the lowest total entropy relative to an affine transformation. The unified method was relatively insensitive to the choices of frequency cutoff or regularization. In addition, the unified method provided greater values of total entropy relative to the standard method. One outlier was excluded from the figure (unified method) because the total entropy for this subject was consistently more than three fold lower than the first quartile of the diabetic group. (* Denotes default parameters for nonlinear transformation in SPM).

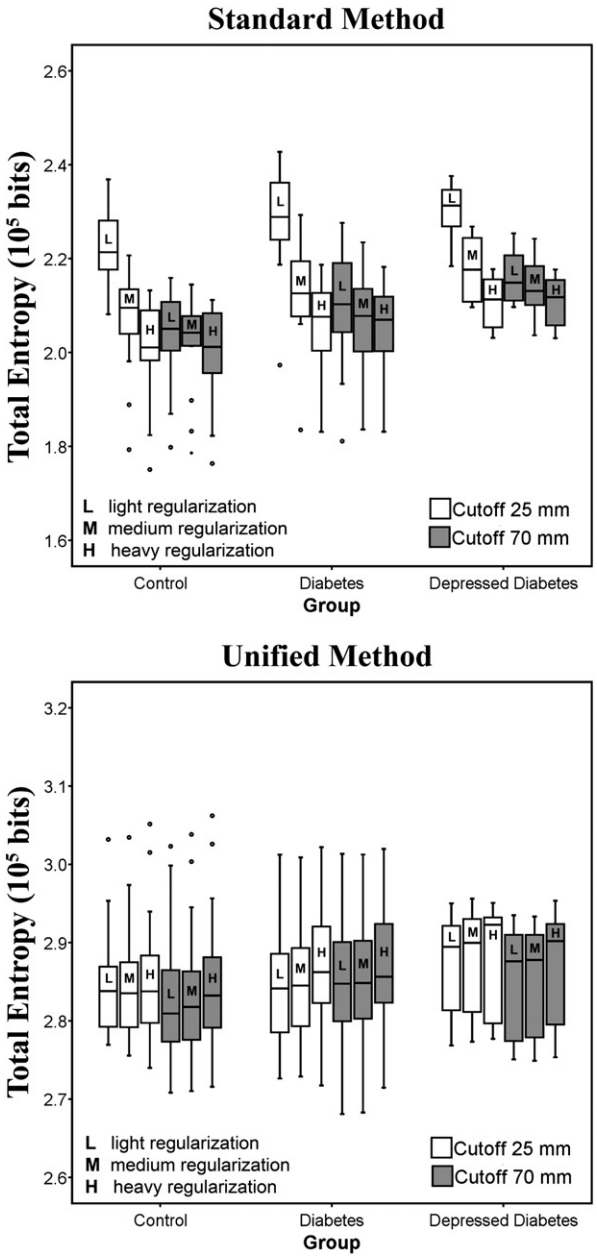

Fig. 2. Residual variability (i.e., total entropy) for normalizations performed by varying more than one parameter at a time: frequency cutoff (25 mm* or 70 mm) and regularization (light, medium* or heavy), for both SPM5 methods (top graph: standard, bottom graph: unified). Regularization had little effect when applying a larger frequency cutoff. The unified model was relatively insensitive to the choice of frequency cutoff or regularization. The unified method provided greater values of total entropy relative to the standard method. One outlier was excluded from the figure (unified method) because the total entropy for this subject was consistently more than three fold lower than the first quartile of the diabetic group. (* Denotes default parameters for nonlinear transformation in SPM).

mid-life/elderly data set. Nonparametric testing for differences in entropy across parameter settings were statistically significant for each of the three groups (controls, diabetics and depressed diabetics), with a maximum observed significance of $p=0.008$ for choice of nonlinear frequency cutoff, $p<0.001$ for choice of nonlinear regularization and $p=0.013$ for nonlinear iterations. In addition, individually optimal parameters: larger nonlinear frequency cutoff, higher nonlinear regularization and fewer nonlinear iterations provide significantly lower residual variability than the default parameters using the standard approach in SPM5. Table 2 summarizes nonparametric results obtained for comparison of the spatial normalization determined for the minimum total entropy data relative to the default values. All comparisons were statistically significant. It should be noted that the p-values from the nonparametric tests, comparing minimum total entropy to the default value, should be interpreted with caution since these values are not corrected for multiple comparisons.

SPM5 Unified Method (UM)

Nonlinear transformation gave lower total entropy when compared to affine transformation when using the unified approach. This finding held true for all three groups. The difference in mean total entropy value between an affine and nonlinear transformation for the unified method was between 6 and 9%.

Warp frequency cutoff (UM). Nonlinear transformation with a frequency cutoff of 70 mm resulted in smaller total entropy for all three groups, when compared to the default 25 mm (top, Fig. 1A). However, the difference in mean total entropy value between a smaller and larger frequency cutoff was negligible (0.14–0.80 percent). The mean entropy for a frequency cutoff of 25 mm for controls, diabetics and depressed diabetics was 2.85×10^5(s.d.= 0.08), 2.75×10^5 (s.d.=0.41) and 2.88×10^5 (s.d.=0.07) bits, respectively and for a cutoff of 70 mm was 2.84×10^5 (s.d.=0.10), 2.75×10^5 (s.d.=0.38) and 2.85×10^5 (s.d.=0.07) bits, respectively. A smaller mean entropy value for the diabetics was because of an outlier (2.85×10^5 bits without the outlier for both frequency cutoffs). This outlier was excluded from Fig. 1A (top) because the

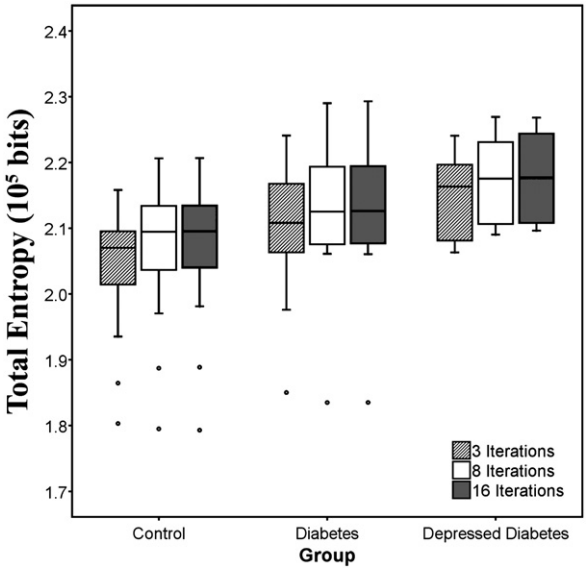

Fig. 3. Residual variability (i.e., total entropy) for normalization performed by varying the number of nonlinear iterations (3, 8 or 16* iterations), while setting all other parameters to the default using the SPM5 standard approach. Fewer number of nonlinear iterations can provide significantly lower residual variability but a greater number may be needed to achieve finer matching of more complex deformations. (* Denotes default parameters for nonlinear transformation in SPM5).

Table 2
Nonparametric tests comparing lowest total entropy with default parameter for the standard method in SPM5

	SPM5 standard method default parameter versus parameter with smallest total entropy		
	Nonlinear frequency cutoff	Nonlinear regularization	Nonlinear iterations
	25 mm* versus 70 mm	medium* versus heavy	16* versus 3
Control			
p-value	$p=0.001$	$p=0.001$	$p=0.002$
Diabetes			
p-value	$p=0.001$	$p<0.001$	$p=0.013$
Depressed diabetes			
p-value	$p=0.012$	$p=0.012$	$p=0.012$

*Denotes default parameters in SPM.

total entropy for this subject was consistently more than three fold lower than the first quartile of the diabetic group.

Warping regularization (UM). The total entropy results show that the light regularization gave smaller residual variability for all three groups. Results are shown on the top of Fig. 1B. The mean entropy for medium regularization for controls, diabetics and depressed diabetics was 2.85×10^5(s.d.=0.08), 2.75×10^5 (s.d.=0.41) and 2.88×10^5 (s.d.=0.07) bits, respectively and the mean entropy for light regularization for controls, diabetics and depressed diabetics was 2.85×10^5 (s.d.=0.07), 2.71×10^5 (s.d.=0.54) and 2.87×10^5 (s.d.=0.07) bits, respectively. A smaller mean entropy value for the diabetics was because of an outlier (2.85×10^5 and 2.84×10^5 bits without the outlier for medium and light regularization respectively). This outlier was excluded from Fig. 1B (top) because the total entropy for this subject was consistently more than three fold lower than the first quartile of the diabetic group.

Combination of nonlinear frequency cutoff and nonlinear regularization (UM). Fig. 2 (bottom) shows that spatial normalization in the unified model is generally insensitive to the choice of parameter settings, when combining different levels of nonlinear frequency cutoff and nonlinear regularization. One outlier was excluded because the total entropy for this subject was consistently more than three fold lower than the first quartile of the diabetic group.

Nonparametric statistical results. There were no differences detected in residual variability when parameter settings change in the nonlinear transformation using the unified approach, with the exception of different levels of regularization for the diabetics ($p=0.01$). Results are not shown.

Standard method versus unified method

An affine transformation yielded the smallest total entropy for the standard approach, when compared to a nonlinear transformation. In contrast, nonlinear normalization provided the lowest residual variability for the unified method. The total entropy results suggest that the unified method provides larger total entropy relative to the standard method. Both methods yielded similar number of outliers; however, they identified different subjects with the exception of one subject. The reason that both methods identified the same outlier was because the subject was not optimally positioned in the field of view. Total entropy results also show that the unified method is insensitive to parameter variation.

SPM maps

Our results indicate that the use of different parameter settings for the standard approach may alter the SPM maps. The comparison of frequency cutoffs (25 mm and 70 mm) yielded statistically significant differences in cortical white matter (primarily gyri) with few gray matter differences (insula and temporal gyri). Comparison of medium and heavy regularization indicated significant differences, about equally, in white matter (fusiform and frontal gyri) and gray matter (frontal gyri, anterior cingulate, claustrum and lentiform nucleus). Finally, the comparison of iteration number (16 vs. 3) yielded significant differences in gyral areas of the frontal, temporal, and occipital lobes and the only difference noted for CSF (lateral ventricle/sub-lobar). SPM analyses that compared different levels of regularization for the unified method did not detect statistically significant differences.

Discussion

In this comparative study, we used total entropy as a performance measure to assess the effects of different parameter settings on the residual variability associated with the spatial normalization of mid-life/elderly MR imaging data (healthy controls or type 2 diabetics). Overall, we found the standard method of normalization in SPM5 to be sensitive to changes in nonlinear frequency cutoff, nonlinear regularization and number of nonlinear iterations, while the unified method was relatively insensitive to such parameter variations.

For the standard method in SPM5, the total entropy results indicated lower residual variability for the affine transformation than for all nonlinear transformations. It is possible for a larger frequency cutoff to yield less residual variability in the nonlinear normalization, relative to a smaller cutoff. This is consistent with the notion that as more basis functions are used, it is possible to match more distortions because higher frequency deformations can be modeled (Salmond et al., 2002). As expected, as the regularization increases, the total entropy decreases and is closer in value to the entropy results for the affine transformation. It is possible that a greater regularization could allow better matching because the penalty increases for quickly changing transformations. However, regularization of larger frequency cutoff had little effect on the residual variability of the normalization. The entropy results for the standard method also indicated that good spatial normalization might be achieved with only a few iterations of the nonlinear warping process. The lowest residual variability for the standard nonlinear spatial normalization of mid-life/elderly image data was achieved by using "heavy" regularization, with all other parameters set at the default value. Analogous comparisons were performed in SPM2 and these results were very similar to those reported herein for the SPM5 standard method (results not shown).

For the unified method in SPM5, the total entropy results indicated lower residual variability for the nonlinear transformations than for the affine transformation. In contrast to the standard method, variations in frequency cutoff and/or regularization had little effect on the normalization and the residual variability determined using the SPM5 unified approach. The unified method performed well for the mid-life/elderly image data, when using the default parameters, in a manner consistent with Crinion et al. (2007). These findings are consistent with those of Hellier et al. (2003) who reported better spatial normalization of skull-stripped images using nonlinear normalizations over affine.

It is acknowledged that the lowest total entropy may not necessarily be indicative of the best normalization result. In this work, the standard method provided lower entropy values (1.7 - 2.4×10^5 bits) than the unified method ($2.7–3.3 \times 10^5$ bits), but the latter method provided more stable results across parameter settings. The larger total entropy observed for the unified method, compared to the standard method (Figs. 1 and 2) appeared to result from greater entropy in gray and white matter but not in CSF, based upon the examination of segmentation results across several default settings (data not shown).

We chose to use this measure because it reflected residual variability based upon individual tissue types. Warfield et al. (2001) proposed the use of total entropy to assess image alignment for affine and nonlinear registration algorithms. Robbins et al. (2004) utilized total entropy to assess performance, to tune, and to compare spatial normalization methods. The total entropy measure could be readily applied in this work because all imaging was performed on the same MR scanner using the same protocol. Another measure that has been very useful for assessing differences in registration or deformations is the root mean squared displacement that is based upon differences in voxel distances relative to anatomical landmarks (Crinion et al., 2007). Hellier et al. (2003) also proposed several global and local measures to assess the performance of different nonrigid registration methods. The precision of the spatial normalization in SPM has also been assessed in terms of anatomical landmarks by calculating the standard deviation from the mean position of the landmark (Salmond et al., 2002). An advantage of the total entropy measure is that it does not require anatomical landmark definition, and therefore can be applied by a user who does not have a strong background in neuroanatomy, and no inter-rater reliability assessments of landmark identification is needed.

Technical factors, such as poor positioning of the subject in the scanner or subject movement, can influence the spatial normalization of the standard method and the spatial normalization and segmentation of the unified method, and thus the total entropy. Extreme segmentation failure (extreme outlier) caused the total entropy to be dramatically underestimated. The dependence of the total entropy on the segmentation process was further evaluated by examining the segmented image data (gray matter, white matter and CSF) for both standard and unified SPM5 methods (several default settings). Pearson's correlations were performed to explore potential relationships between age (degree of atrophy) and total entropy for the three tissue types. The results were ambiguous across the subject groups with the only significant result indicated for diabetics for which greater age was associated with greater CSF entropy (more CSF is expected with greater atrophy) but less gray matter and white matter entropy (data not shown). Finally, as stated above, gray and white matter entropies were greater for the unified method than for the standard method, while CSF entropies were similar for both methods.

The SPM analyses of the data processed using the standard approach indicated that the frequency cutoff resulted in normalization differences most often observed in cortical white matter (frontal and temporal gyri) and less often in gray matter (temporal gyri). Differences in regularization warping influenced both gray and white matter of frontal and temporal cortices. The SPM analysis also indicates that the number of iterations might significantly affect the warping of gyral areas in cortex and along the lateral ventricle (areas adjacent to and including CSF).

Total entropy results and SPM analyses suggest that the best parameters for nonlinear spatial normalization of mid-life/elderly image data to the MNI template, when applying the standard approach, correspond to a smaller cutoff (25 mm), heavy regularization, and the default number of nonlinear iterations (16). A smaller frequency cutoff may allow for better matching of deformations, heavy regularization could limit distortions that might occur when warping mid-life/elderly image data to the young template, and sixteen iterations because these may improve the normalization in areas adjacent to or containing CSF. On the other hand, when applying the unified approach, the default parameters were the best for spatial normalization of mid-life/elderly image data to the MNI priors, given the apparent lack of sensitivity of the method to variations in the parameter settings. In contrast to the standard method, it is possible that the total entropy measure may not be a sensitive indicator for the assessment of parameter variations in the unified method.

For clinical research applications, it can be important to try to match the normalization method with the research question. The preferred normalization would be one that provides a good compromise between the extent to which an individual's MR image is adjusted *and* optimal matching of the brain to the standard template. The normalization-of-choice would allow for the detection of pathology-related changes rather than differences that may exist between the individual's MR and the template. If age-related changes are of interest, then one would want to apply a normalization that would modify the individual's MR image least, while providing the best normalization in areas where age-related group differences are expected (e.g., frontal cortex or ventricles/CSF).

These findings are relevant for studies of structural brain alterations that may occur in normal aging, chronic medical conditions, neuropsychiatric disorders, and neurodegenerative disorders. Future studies will extend this work in the context of subject- or disease-specific templates/tissue priors.

Acknowledgments

This work was supported by NIH grants (K01 MH01976, P30 DK046205, P01 AG025204, P30 MH52247, R01 DK39629, R01 MH59945, MO1-RR000056, R01 MH070729). The authors are deeply indebted for the mentorship and recruitment support provided by the University of Pittsburgh Obesity and Nutrition Research Center (Dr. David E. Kelley), Intervention Research Center for Late-life Mood Disorders (Dr. Charles F Reynolds, III), Dr. Christopher M. Ryan, and Dr. Sigrid A. Hagg. We thank Dr. Carolyn C. Meltzer for sharing MR data of 4 elderly controls. We also thank the MR and PET research staff, M. Geckle, M. Bechtold, and S. Hulland for their help with these studies. We also thank Drs.Steven DeKosky and William Klunk for their helpful comments.

References

Ashburner, J., Friston, K.J., 1999. Nonlinear Spatial Normalization using Basis Functions. Hum. Brain Mapp. 7, 254–266.

Ashburner, J., Friston, K.J., 2005. Unified Segmentation. NeuroImage 26, 839–851.

Cover, T.M., Thomas, J.A., 2006. Elements of Information Theory, Second Edition. John Wiley & Sons, Inc.

Crinion, J., Ashburner, J., Leff, A., Brett, M., Price, C., Friston, C., 2007. Spatial normalization of lesioned brains: Performance evaluation and impact on fMRI analyses. NeuroImage 37, 866–875.

Crivello, F., Schormann, T., Tzourio-Mazoyer, N., Roland, P.E., Zilles, K., Mazoyer, B.M., 2002. Comparison of spatial normalization procedures and their impact on functional maps. Hum. Brain Mapp. 16 (4), 228–250.

Gispert, J.D., Pascau, J., Reig, S., Martinez-Lazaro, R., Molina, V., Garcia-Barreno, P., Desco, M., 2003. Influence of the normalization template on

the outcome of statistical parametric mapping of PET scans. NeuroImage 19, 601–612.

Hellier, P., Barillot, I., Corouge, I., Gibaud, B., Le Goualher, G., Collins, D.L., Evans, A., Malandain, G., Ayache, N., Christensen, G.E., Johnson, H.J., 2003. Retrospective Evaluation of Intersubject Brain Registration. IEEE Trans. Med. Imag. 22 (9), 1120–1130.

Hosaka, K., Ishii, K., Sakamoto, S., Sadato, N., Fukuda, H., Kato, T., Sugimura, K., Senda, M., 2005. Validation of anatomical standardization of FDG PET images of normal brain: comparison of SPM and NEUROSTAT. Eur. J. Nucl. Med. Mol. Imaging 32 (1), 92–97.

Meyer, J.H., Gunn, R.N., Myers, R., Grasby, P.M., 1999. Assessment of Spatial Normalization of PET Ligand Images Using Ligand-Specific Templates. NeuroImage 9, 545–553.

Price, J.C., Kelley, D.E., Ryan, C.M., Meltzer, C.C., Drevets, W.C., Mathis, C.A., Mazumdar, S., Reynolds, C.F., 2002. Evidence of Increased Serotonin-1A Receptor Binding in Type 2 Diabetes: A Positron Emission Tomography Study. Brain Res. 927 (1), 97–103.

Price, J.C., Kelley, D.E., Hagg, S.A., Meltzer, C.C., Ryan, C.M., Mazumdar, S., Mathis, C.A., Reynolds, C.F., 2003. Measurement of serotonin-1A receptor binding in diabetes and depression. J. Nucl. Med. 44 (5), S896.

Robbins, S., Evans, A.C., Collins, D.L., Whitesides, S., 2004. Tuning and comparing spatial normalization methods. Med. Image Anal. 8, 311–323.

Salmond, C.H., Ashburner, J., Vargha-Khadem, F., Connelly, A., Gadian, D.G., Friston, K.J., 2002. Technical Note: The Precision of Anatomical Normalization in the Medial Temporal Lobe Using Spatial Basis Functions. NeuroImage 17, 507–512.

Sugiura, M., Kawashima, R., Sadato, N., Senda, M., Kanno, I., Oda, K., Sato, K., Yonekura, Y., Fukuda, H., 1999. Anatomic Validation of Spatial Normalization Methods for PET. J. Nucl. Med. 40 (2), 317–322.

Warfield, S.K., Rexilius, J., Huppi, P.S., Inder, T.E., Miller, E.G., Wells III, W.M., Zientara, G.P., Jolesz, F.A., Kikinis, R., 2001. A binary entropy measure to assess nonrigid registration algorithms. Medical Image Computing and Computer-Assisted Intervention. Lecture Notes in Computer Science Proceedings of the 4th International Conference on Medical Image Computing and Computer-Assisted Intervention, vol. 2208. Springer, pp. 266–274.

Wellcome Department of Imaging Neuroscience, 1994–2007. Statistical Parametric Mapping Software, London, UK. http://www.fil.ion.ucl.ac.uk/spm/.

Wu, M., Carmichael, O., Lopez-Garcia, P., Carter, C., Aizenstein, H.J., 2006. Quantitative Comparison of AIR, SPM, and the Fully Deformable Model for Atlas-Based Segmentation of Functional and Structural MR Images. Hum. Brain Mapp. 27, 747–754.

BIBLIOGRAPHY

Ashburner, J., Friston K.J., 1999. Nonlinear Spatial Normalization using Basis Functions. *Human Brain Mapping*, 7:254-266.

Ashburner, J., Friston, K.J., 2005. Unified segmentation. *NeuroImage*, 26: 839 – 851.

Beta amyloid. (2008). In *Wikipedia, the free encyclopedia*. Retrieved November 15, 2008, from http://en.wikipedia.org/wiki/Amyloid_beta.

Bittner, D., Grön, G., Schirrmeister, H., Reske, S.N., Riepe, M.W., 2005. [^{18}F]-FDG-PET in Patients with Alzheimer's Disease: Marker of Disease Spread. *Dementia and Geriatric Cognitive Disorders*, 19(1): 24-30.

Bookstein, F.L., 1991. Morphometric Tools for Landmark Data: Geometry and Biology. New York: Cambridge University Press.

Bookstein, F.L., 1989. Principal warps: Thin-plate splines and the decomposition of deformations. *IEEE Transactions on Pattern Analysis and Machine Intelligence*, 11(6): 567-585.

Cover, T. M., Thomas, J. A., 2006. Elements of Information Theory, Second Edition. John Wiley & Sons, Inc.

Crinion, J., Ashburner, J., Leff, A., Brett, M., Price, C., Friston, K., 2007. Spatial normalization of lesioned brains: Performance evaluation and impact on fMRI analyses. *NeuroImage*, 37: 866-875.

Crivello, F., Schormann, T., Tzourio-Mazoyer, N., Roland, P.E., Zilles, K., Mazoyer, B.M., 2002. Comparison of spatial normalization procedures and their impact on functional maps. *Human Brain Mapping*, 16(4): 228-250.

Drineas, P., Frieze, A., Kannan, R., Vempala, S., Vinay, V., 2004. Clustering Large Graphs via the Singular Value Decomposition, *Machine Learning*, 56: 9-33.

Evans, A.C., Dai, W., Collins, L., Neelin, P., Marrett, S., 1991. Warping of a computerized 3-D atlas to match brain image volumes for quantitative neuroanatomical and functional analysis. *SPIE Image Processing*, 1445: 236-246.

Folstein, M., Folstein, S., McHugh, P.R., 1975. "Mini-mental state": A practical method for grading the cognitive state of patients for the clinician. *Journal of Psychiatric Research*, 12 (3): 189-198.

Gispert, J.D., Pascau, J., Reig, S., Martinez-Lazaro, R., Molina, V., Garcia-Barreno, P., Desco, M., 2003. Influence of the normalization template on the outcome of statistical parametric mapping of PET scans. *NeuroImage*, 19: 601-612.

Hamacher, K., Coenen, H.H., Stocklin, G., 1986. Efficient stereospecific synthesis of no-carrier-added 2-[^{18}F]fluoro-2-deoxy-D-glucose using aminopolyether supported nucleophilic substitution. *Journal of Nuclear Medicine,* 27(2): 235-238.

Hastie, T.J. and Tibshirani, R.J., 1990. Generalized Additive Models, Monographs on Statistics and Applied Probability 43. Chapman and Hall.

Hoffman, J.M., Guze, B.H., Baxter, L.R., Mazziotta, J.C., Phelps, M.E., 1989. [^{18}F]-Fluorodeoxyglucose (FDG) and Positron Emission Tomography (PET) in Aging and Dementia. *European Neurology*, 29(3): 16-24.

Hosaka, K, Ishii, K., Sakamoto, S., Sadato N., Fukuda, H., Kato, T., Sugimura, K., Senda, M., 2005. Validation of anatomical standardization of FDG PET images of normal brain: comparison of SPM and NEUROSTAT. *European Journal of Nuclear Medicine and Molecular Imaging*, 32(1).

Johnson, H.J., Christensen, G.E., 2002. Consistent Landmark and Intensity-Based Image Registration. *IEEE Transactions of Medical Imaging*. 21(5): 450 – 461.

Klunk, W.E., Engler, H., Nordberg, A., Wang, Y., Blomqvist, G., Holt, D.P., Bergstrom, M., Savitcheva, I., Huang, G.F., Estrada, S., Ausen, B., Debnath, M.L., Barletta, J., Price, J.C., Sandell, J., Lopresti, B.J., Wall, A., Koivisto, P., Antoni, G., Mathis, C.A., Langstrom, B., 2004. Imaging brain amyloid in Alzheimer's disease with Pittsburgh Compound-B. *Annals of Neurology*, 55(3): 306-19.

Klunk, W.E., Price, J.C., Mathis, C.A., Tsopelas, N.D., Lopresti, B.J., Ziolko, S.K., Bi, W., Hoge, J.A., Cohen, A.D., Ikonomovic, M.D., Saxton, J.A., Snitz, B.E., Pollen, D.A., Moonis, M., Lippa, C.F., Swearer, J.M., Johnson, K.A., Rentz, D.M., Fischman, A.J., Aizenstein, H.J., DeKosky, S.T. 2007. Amyloid Deposition Begins in the Striatum of Presenilin-1 Mutation Carriers from Two Unrelated Pedigrees. *The Journal of Neuroscience*, 27(23): 6174-6184.

Lobaugh, N.J., West, R., McIntosh, A.R., 2001. Spatiotemporal analysis of experimental differences in event-related potential data with partial least squares. *Psychophysiology*, 38: 517-530.

Logan, J., Fowler, J.S., Volkow, N.D., Wang, G.-J., Ding, Y.-S., Alexoff, D.L., 1996. Distribution volume ratios without blood sampling from graphical analysis of PET data. *Journal of Cerebral Blood Flow & Metabolism*, 16: 834–840.

Lopresti, B.J., Klunk, W.E., Mathis, C.A., Hoge, J.A., Ziolko, S.K., Lu, X., Meltzer, C.C., Schimmel, K., Tsopelas, N.D., DeKosky, S.T., Price, J.C., 2005. Simplified Quantification of Pittsburgh Compound B Amyloid Imaging PET Studies: A Comparative Analysis. *Journal of Nuclear Medicine*, 46(12): 1959-1972.

McIntosh, A.R., Lobaugh, N.J., 2004. Partial least squares analysis of Neuroimaging data: applications and advances. *NeuroImage*, 23:S250-S263.

McIntosh, A.R., Bookstein, F.L., Haxby, J.V., Grady, C.L., 1996. Spatial Pattern Analysis of Functional Brain Images Using Partial Least Squares. *NeuroImage*, 3: 143-157.

Meyer, J.H., Gunn, R.N., Myers, R., Grasby, P.M., 1999. Assessment of Spatial Normalization of PET Ligand Images Using Ligand-Specific Templates. *NeuroImage*, 9:545-553.

Minoshima, S., Frey, K.A., Koeppe, R.A., Foster, N.L., Kuhl, D.E., 1995. A Diagnostic Approach in Alzheimer's Disease Using a Three-dimensional Stereotactic Surface Projections of Fluorine-18-FDG-PET. *The Journal of Nuclear Medicine*, 36(7): 1238-1248.

Nestor, P.G., O'Donnell, B.F., McCarley, R.W., Niznikiewicz, M., Barnard, J., Shen, Z.J., Bookstein, F.L., Shenton, M.E., 2002. A new statistical method for testing hypotheses of neuropsychological/MRI relationships in schizophrenia: partial least squares analysis. *Schizophrenia Research*, 53: 57-66.

Positron emission tpomography. (2008). In *Wikipedia, the free encyclopedia*. Retrieved November 15, 2008, from http://en.wikipedia.org/wiki/Positron_emission_tomography.

Price, J.C., Klunk, WE., Lopresti, B.J., Lu, X., Hoge, J.A., Ziolko, S.K., Holt, D.P., Meltzer, C.C., DeKosky, S.T., Mathis, C.A., 2005. Kinetic modeling of amyloid binding in humans using PET imaging and Pittsburgh Compound-B. *Journal of Cerebral Blood Flow & Metabolism*, 25: 1528-1547.

Price, J.C., Kelley, D.E., Hagg, S.A., Meltzer, C.C., Ryan, C.M., Mazumdar, S., Mathis, C.A., Reynolds, C.F., 2003. Measurement of serotonin-1A receptor binding in diabetes and depression. *Journal of Nuclear Medicine*, 44(5):S896.

Price, J.C., Kelley, D.E., Ryan, C.M., Meltzer, C.C., Drevets, W.C., Mathis, C.A., Mazumdar, S., Reynolds, C.F.., 2002. Evidence of Increased Serotonin-1A Receptor Binding in Type 2 Diabetes: A Positron Emission Tomography Study. *Brain Research*, 927(1):97-103.

Radioactive tracer. (2008). In *Wikipedia, the free encyclopedia*. Retrieved November 15, 2008, from http://en.wikipedia.org/wiki/Radioactive_tracer.

Robbins, S., Evans, A.C., Collins, D.L., Whitesides, S., 2004. Tuning and comparing spatial normalization methods. *Medical Image Analysis*, 8: 311-323.

Rohr, K., Stiehl, H.S., Sprengel, R., Buzug, T.M., Weese, J., Kuhn, M.H. 2001. Landmark-Based Elastic Registration Using Approximating Thin Plate Splines. *IEEE Transactions on Medical Imaging*. 20(6): 526 – 534.

Rohr, K., Stiehl, H.S., Sprengel, R., Beil, W., Buzug, T.M., Weese, J., Kuhn, M.H. 1996. Point-Based Elastic Registration of Medical Image Data Using Approximating Thin Plate Splines. *Visualization of Medical Computing*, Springer Verlag. 297 – 306.

Rosario, B.L., Ziolko, S.K., Weissfeld, L.A., Price, J.C., 2008. Assessment of parameter settings for SPM5 spatial normalization of structural MRI data: Application to type 2 diabetes. *NeuroImage*, 41: 363-370.

Salmond, C.H., Ashburner, J., Vargha-Khadem, F., Connelly, A., Gadian, D.G., Friston, K.J., 2002. Technical Note: The Precision of Anatomical Normalization in the Medial Temporal Lobe Using Spatial Basis Functions. *NeuroImage*, 17:507-512.

Silverman, D., 2004. Brain ^{18}F–FDG PET in the Diagnosis of Neurodegenerative Dementias: Comparison with Perfusion SPECT and with Clinical Evaluations Lacking Nuclear Imaging. *Journal of Nuclear Medicine*, 45(4): 594-607.

Spears, J.R., Greer, P.J., Ziolko, S.K., Aizenstein, H.J., Carmichael, O., Becker, J.T., Meltzer, C.C., 2005. Construction and evaluation of an age-specific neurological template. *NeuroImage*, 26 (S1), S47.

Sugiura, M., Kawashima, R., Sadato, N., Senda, M., Kanno, I., Oda, K., Sato, K., Yonekura, Y., Fukuda, H., 1999. Anatomic Validation of Spatial Normalization Methods for PET. *Journal of Nuclear Medicine*, 40(2): 317-322.

The Mathworks – MATLAB, 1994-2008. MATLAB R2008a, http://www.mathworks.com/.

The R Project for Statistical Computing, 1997-2007. R Software, http://www.r-project.org/.

Wahba, G. 1990. Spline Models for Observational Data. Society for Industrial and Applied Mathematics. Philadelphia, Pennsylvania.

Warfield, S.K., Rexilius, J., Huppi, P.S., Inder, T.E., Miller, E.G., Wells III, W.M., Zientara, G.P., Jolesz, F.A., Kikinis, R., 2001. A binary entropy measure to assess nonrigid registration algorithms. *Medical Image Computing and Computer-Assisted Intervention. Lecture Notes in Computer Science*, Springer.

Watson, C.C., 2000. New, faster, image-based scatter correction for 3D PET. *IEEE Transactions of Nuclear Science*, 47: 1587-1594.

Wellcome Department of Imaging Neuroscience., 1994-2007. Statistical Parametric Mapping Software, London, UK. http://www.fil.ion.ucl.ac.uk/spm/.

Wilson, A.A., Garcia, A., Chestakova, A., Kung, H., Sylvain Houle, S., 2004. A rapid one-step radiosynthesis of the β-amyloid imaging radiotracer *N*-methyl-[^{11}C]2-(4´-methylaminophenyl)-6-hydroxybenzothiazole ([^{11}C]-6-OH-BTA-1). *Journal of Labelled Compounds and Radiopharmaceuticals*, 47: 679–682.

Wold, H., 1975. Soft modelling by latent variables: the nonlinear iterative partial least squares(nipals) approach. *Perspectives in Probability and Statistics, In Honor of M.S. Bartlett*:117-144.

Wu, M., Carmichael, O., Lopez-Garcia, P., Carter, C. and Aizenstein, H.J., 2006. Quantitative Comparison of AIR, SPM, and the Fully Deformable Model for Atlas-Based Segmentation of Functional and Structural MR Images. *Human Brain Mapping*, 27: 747-754.

Xie, X., Chung, M.K., Wahba, G., 2006. Magnetic Resonance Image Segmentation with Thin Plate Spline Thresholding. Technical Report NO. 1105, Univerity of Wisconsin.

Xu, L., Mazumdar, S., Price, J., 2007. Covariate adjustment in partial least squares (PLS) regression for the extraction of the spatial-temporal pattern from positron emission tomography data. *Statistical Methodology*, 4: 44-63.

Ziolko, S.K., Weissfeld, L.A., Klunk, W.E., Mathis, C.A., Hoge, J.A., Lopresti, B.J., DeKosky, S.T., Price, J.C., 2006. Evaluation of voxel-based methods for the statistical analysis of PIB PET amyloid imaging studies in Alzheimer's disease. *NeuroImage*, 33(1): 94-102.